NASA Contractor Report 3757

Surface Topographical Changes Measured by Phase-Locked Interferometry

James L. Lauer and Simon S. Fung

GRANT NAG3-222
JANUARY 1984

NASA

NASA Contractor Report 3757

Surface Topographical Changes Measured by Phase-Locked Interferometry

James L. Lauer and Simon S. Fung
Rensselaer Polytechnic Institute
Troy, New York

Prepared for
Lewis Research Center
under Grant NAG3-222

National Aeronautics
and Space Administration

**Scientific and Technical
Information Office**

1984

CONTENTS

SUMMARY

An electronic optical laser interferometer capable of resolving depth differences of as low as 30 Å and planar displacements of 6000 Å was constructed for the examination of surface profiles of bearing surfaces without physical contact. This instrument was used to determine topological chemical reactivity by applying a drop of dilute alcoholic hydrochloric acid and measuring the profile of the solid surface before and after application of this probe. It was found that scuffed bearing surfaces reacted much faster than virgin ones but that bearing surfaces exposed to lubricants containing an organic chloride reacted much more slowly. In a separate series of experiments, a number of stainless steel plates were heated in a nitrogen atmosphere to different temperatures and their reactivity examined later at ambient temperature. The change of surface contour as a result of the probe reaction was found to follow an Arrhenius-type relation with respect to heat treatment temperature. In another experiment, the contact area of the plate of a ball/plate (both consisting of hardened M-50 steel) sliding elastohydrodynamic contact run on trimethylolpropane triheptanoate with or without the additives dioctyldiphenylamine (DODPA), phenyl-alpha-naphthylamine (PANA), benzotriazole (BTZ), and tricresyl phosphate (TCP) individually and collectively was optically profiled periodically with the phase-locked interference microscope, both before and after exposure to alcoholic hydrochloric acid. As scuffing was approached the change of profile within the contact region changed much more rapidly by the acid probe and assumed a constant high value after scuffing. A new nonetching metallurgical phase was found in the scuff mark, which was

apparently responsible for the high reactivity. Soaking the metal surfaces in the various lubricants before running was found to affect the subsequent reactivity. Based on the above findings, it would appear that this type of examination could be used for screening of potentially scuff-resistant materials.

PART 1

INTRODUCTION

When nonconforming solid surfaces separated by a lubricant are in relative motion under increasing loads, the bulk temperature gradually increases and the lubricant film thickness decreases. At some point, the surfaces will begin to interact mechanically. At first, the peaks of the highest asperities will be reduced and the surfaces will become smoother. This interaction is an essential part of normal "run-in." At higher loads, scoring occurs, manifested by grooves and ridges in the surface oriented in the sliding direction. At still higher loads, a sudden failure may occur, which is called "scuffing." The scoring and scuffing events are often coincident and many authors have been using these terms interchangeably.

Because scuffing is likely to be catastrophic and without warning, measures were designed to postpone it or avoid it. Since welding of the contacting surfaces has been considered an essential part of scuffing, these measures usually entail the formation of interposed layers. For example, the use of extreme pressure (EP) lubricant additives is thought to result in the formation of renewable coatings of metal sulfides, chlorides, or phosphates preventing the welding. A durable coating of the surfaces with thin, hard, inert layers could also avert scuffing for the same reason and could work even without a lubricant - an added advantage under severe conditions, when the lubricant is subject to thermal breakdown.

Although the mechanism of scuffing is not yet fully understood, a temperature criterion is commonly postulated. The best known

is the "total temperature" of Blok [16], which consists of the bulk temperature of the metal parts and the instantaneous surface temperature rise of the surface area of contact. Others correlated scuffing failure primarily with chemical activity which, of course, is itself strongly influenced by temperature [24]. Implicitly, the assumption has been made that chemical reaction would take place primarily above the characteristic ("total") temperature between metal and lubricant components. Could it be that portions of metal surfaces exposed to temperatures above the characteristic temperature are inherently more reactive at any temperature?

An optical interferometer capable of resolving depth difference as low as 30 Å and planar displacements of 6000 Å became a powerful tool in an attempt to answer this question. Since vacuum is not required, we could carry out probe microreactions on neat and scuffed areas and compare the resulting changes of surface profile. As reactions are happening much faster at a microscale, the time it takes to perform the experiments is significantly cut down. Both titanium-nitride-coated and uncoated bearing balls before and after use in this way were examined and were compared with subsequent scanning electron photomicrographs. Dilute alcoholic hydrochloric acid is used as a probe to induce chemical changes. Metal surfaces heated to known temperatures were examined for reference. The results point to changes caused by the heat treatment, which produced chemical reactivity changes even at ambient temperature and likely mechanism for the absence of scuffing with titanium-nitride-coated balls.

Another series of experiments were performed with a typical military lubricant and the M-50 bearing steel. A lubricated ball/plate bearing contact was set up and run long enough until scuffing occurred. The plate was removed at known intervals before scuffing and the reactivity of the contact region towards diluted hydrochloric acid was determined at room temperature.

The same lubricant with different additives was also used in the same experiment and their reactivity studied. The effect of soaking the bearing surfaces prior to contact operation was also investigated. Originally, this was done to pursue some of the observations, reported by Shafrin [23], on surfaces soaked by tricresyl phosphate (TCP) which is one of the additives in the lubricant. The surfaces were found to undergo some changes which might have some implication on how TCP works as an anti-wear additive.

A metallurgically nonetching phase was also found at the scuffed area, and it may be similar or the same as that reported by Rogers [18]. The same phase may be the same material as what was observed in our experiment

PART 2

HISTORICAL REVIEW

2.1 Definition of Scuffing

There are a number of definitions for scuffing and they are somewhat confusing. The one that has been widely accepted is "gross damage characterized by the formation of local welds between the sliding surfaces" [1]. In some cases, scuffing has the sense "seizure" or "the stopping of a mechanism as the result of interfacial friction." Even though this is rarely encountered in practice, scuffing is a catastrophic type of failure for most lubrication engineers.

Scuffing usually would not cause the entire machine to fail, but it would result in a decrease in performance. In most cases the parts involved have to be replaced. Therefore manufacturers have tried to avoid or eliminate the problem. However, the problems have largely been solved by experience or trial-and-error. Theoretical understanding is still insufficient to allow designers to have an approximate scuffing limit which they can use for novel designs.

2.2 Blok's Postulate

Based on some of the experiences, researchers have come up with a number of empirical criteria for scuffing [2]. The most dominating one is put up by Blok in 1939 [3]. He hypothesized that a characteristic temperature may be allotted to each combination of lubricant and rubbing surfaces. This temperature is independent of load, speed, and bulk temperature. The temperature is called the total temperature. This comprises two components: (1) the bulk temperature of the metal part

which can be measured or estimated, (2) the instantaneous rise in the temperature of the surfaces as they rub against each other. This is known as the flash temperature and is covered in a more detailed form in Part 3. This temperature has a very short duration and it also decays extremely rapidly both in time and in depth into the material, therefore it is exceedingly difficult to be measured and must be estimated.

It is also important to note that the postulate was only intended for straight mineral oil, i.e., no extreme pressure additives.

Many have since then devised experiments in an attempt to correlate between the occurrence of scuffing and the total contact temperature calculated on the basis of an assumed constant coefficient of friction. Lemanski [4] obtained an impressive correlation in his experiment with gears. However, the same data with some additions were later reanalyzed by Kelly and Lemanski [5] with individual estimates of the coefficient of friction for each case and the correlation then became considerably less impressive.

Instead of using gears in their experimentation, Ku [6] was able to predict the scoring load of gears from the result of tests on disks by using the postulate, and their result very much favored the Blok's postulate.

However, the experimental results range from highly consistent with the postulate to contradictory with it. Inconsistent results have been reported by Genkin et al. [7], Cocks and Tallian [8] and many others.

Since there is such a conflict of evidence, the most plausible conclusion would be that Blok's postulate only covers certain ranges of experimental conditions. Bell et al. [9] showed that the total contact

temperature was indeed approximately constant over certain bands of rolling (1.6 - 6.2 ms^{-1}) and sliding (1.6 - 2.5 ms^{-1}) speeds, and that significant deviations were found when experimental conditions were outside this band.

2.3 Frictional Power Intensity

Another criterion is called the frictional power intensity which is the product of the mean Hertzian stress $\bar{p}_H$ and the sliding speed V_s [10]. Bell and Dyson [9] set up another criterion which may have more significant meaning by multiplying the coefficient of friction μ to give the product of the mean shear stress due to friction $\bar{\tau} = \mu\bar{p}_H$ and the sliding speed. The result is the "friction power intensity" which gives the rate of dissipation of energy by friction per unit area of nominal contact.

When Bell and Dyson collected results from a number of authors and plotted the friction power intensity versus the mean rolling speed just before scuffing, they found a wide scattering of data, even though all authors referred to hardened steel surfaces lubricated by mineral oils. This may indicate the limited applicable condition for this criterion as in the case of the Blok's postulate.

2.4 The Minimum Thickness of the Elastohydrodynamic Oil Film

The normal elastohydrodynamic theories assume ideally smooth surfaces and may therefore be expected to break down when the minimum thickness is of or less than the order of the surface roughness. This may conceivably be established as a criterion: scuffing would occur when the oil film thickness is less than the surface roughness. However,

Bell and Dyson [11] reported that the film thickness just before scuffing was independent of initial surface roughness. Since the surface roughness is not monitored (or we still have not developed a technique to do that) during or before the time of scuffing, it is still possible for this idea to become a failure criterion.

PART 3

THEORY

The mathematical basis for phase-locked interferometry and related optical theories will be treated first. Then the theories behind scuffing and the Blok's postulates will be presented.

3.1 Mathematical Basis for Phase-Locked Interferometry

Leiner [12] examined in detail the theory behind phase-locked interferometry. The intensity distribution of the fringes in a two-beam interferometer is illustrated in Figure 3.1 and can be described as follows:

$$I(x,y) = I_1(x,y) + I_2(x,y) + 2\sqrt{I_1(x,y)\,I_2(x,y)}\,\cos\,\delta \qquad (3.1)$$

where

$I_1(x,y)$ ≡ intensity from reference arm

$I_2(x,y)$ ≡ intensity from test arm

$\delta \equiv 2\pi/\lambda$ (optical path difference between the two arms).

Since I_1 and I_2 are the irradiance from the two arms, they are the dc terms; δ can be separated into two parts: the phase due to static interference and the phase due to the oscillating piezoceramic crystal:

$$\delta = \delta_1 + \delta_2 \qquad (3.2)$$

where

$\delta_1(x,y)$ = static phase difference of interferometer arms

$\delta_2(t)$ = sinusoidal varying phase.

For most samples that we measure, δ_1 is basically a random function. Here δ_2 can be further expressed as

$$\delta_2 \equiv A \sin 2\pi ft \qquad (3.3)$$

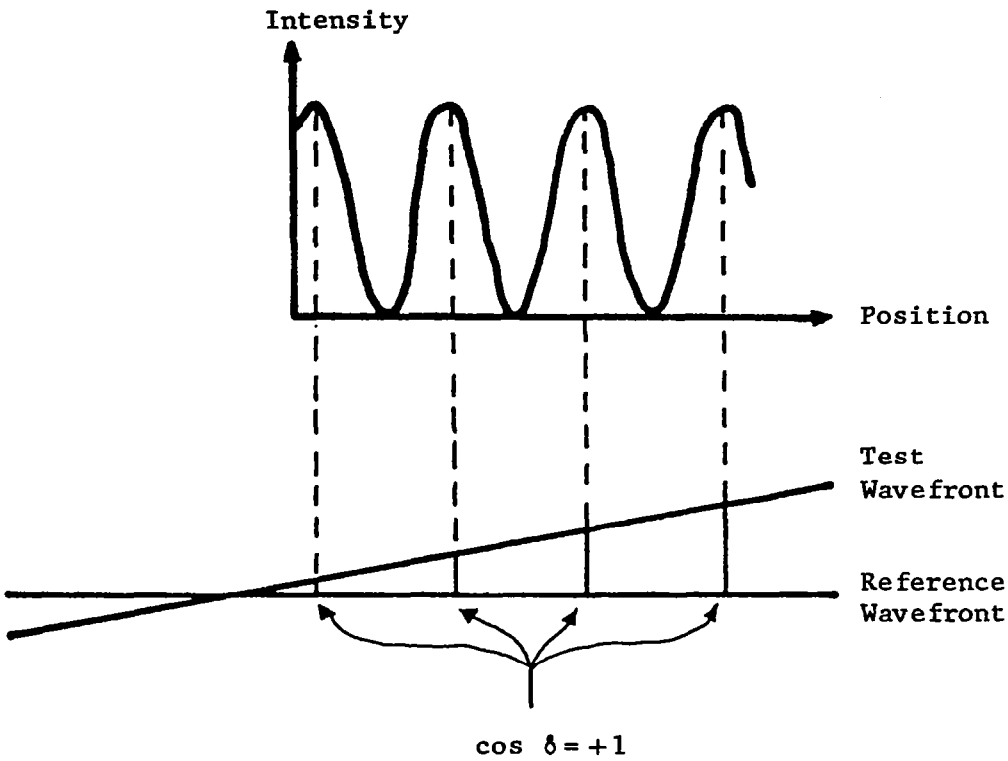

Figure 3.1 Intensity Distribution in Interference Pattern

where A and f are the amplitude and the frequency of the modulating signal, respectively.

Substituting (3.2) and (3.3) into (3.1), we get

$$I(x,y,t) = I_1(x,y) + I_2(x,y) + 2\sqrt{I_1 I_2}\cos(\delta_1 + A \sin 2\pi ft)$$

By expanding the cosine of the sum of two angles, we get

$$I(x,y,t) = I_1(x,y) + I_2(x,y) + 2\sqrt{I_1 I_2}\cos\delta_1 \cos(A\sin 2\pi ft) - \sin\delta_1 \sin(A\sin 2\pi ft).$$

The cosine of a sine and the sine of a sine can be expanded into an infinite series of Bessel functions, so that

$$I(x,y,t) = I_1(x,y) + I_2(x,y) + 2\sqrt{I_1 I_2}\{\cos\delta_1[J_o(A) + 2J_2(A)\cos(4\pi ft) + 2J_4(A)\cos(8\pi ft) + \ldots] - \sin\delta_1[2J_1(A)\sin(2\pi ft) + 2J_3(A)\sin(6\pi ft) + 2J_5(A)\sin(10\pi ft) + \ldots]\}.$$

For the case of phase locking at the maximum or minimum of a fringe, $\delta(x,y) = n\pi$ and therefore the last term goes to zero. It follows that the amplitude of the signal at the driving frequency f is zero and only odd harmonics of f are present. If the detector is not located at either of these extremes, then a signal at the driving frequency will be present with amplitude $4\sqrt{I_1 I_2}J_1(A)\sin\delta(x,y)$.

This term will have either a positive or negative sign if the detector is not locked onto a fringe maxima or minima. A corresponding signal will be generated to drive the signal to the fringe in the actual electronics.

Even though the theory indicates that the detector will lock onto either the bright or the dark fringe, the system only locks onto

the bright fringe. This is because the drak fringes do not generate enough signal at the detector to make it functional.

3.2 Phase Changes on Reflection

3.2.1 Metallic Surface

Consider an interface separating two media, one being dielectric and the other one being a conductor (Figure 3.2). According to the Fresnel formulae [13], the formulae relating to the reflection of a plane monochromatic wave by the metallic medium are

$$r_{12} = \frac{\hat{n}_1 \cos\theta_1 - \hat{n}_2 \cos\theta_2}{\hat{n}_1 \cos\theta_1 + \hat{n}_2 \cos\theta_2} \qquad \text{for transverse electric wave}$$

$$r_{12} = \frac{\frac{1}{\hat{n}_1}\cos\theta_1 - \frac{1}{\hat{n}_2}\cos\theta_2}{\frac{1}{\hat{n}_1}\cos\theta_1 + \frac{1}{\hat{n}_2}\cos\theta_2} \qquad \text{for transverse magnetic wave}$$

where $\hat{n}_1$ and $\hat{n}_2$ are the complex refractive index for medium 1 and 2. The two different states of polarization are defined as:

a) Transverse Electric Polarization (T.E.)
In this case the electric field vector is parallel to the interface and transverse to the plane of incidence which is illustrated in Figure 3.3.

b) Transverse Magnetic Polarization (T.M.)
In this case the magnetic field vector is parallel to the interface and transverse to the plane of incidence.

In this case, since medium 2 is metallic and absorbing, $\hat{n}_2 = n_2 (1 + i\kappa_2)$ and $\hat{n}_1 = n_1$. It is convenient to set

$$\hat{n}_2 \cos\theta_2 = u_2 + iv_2$$

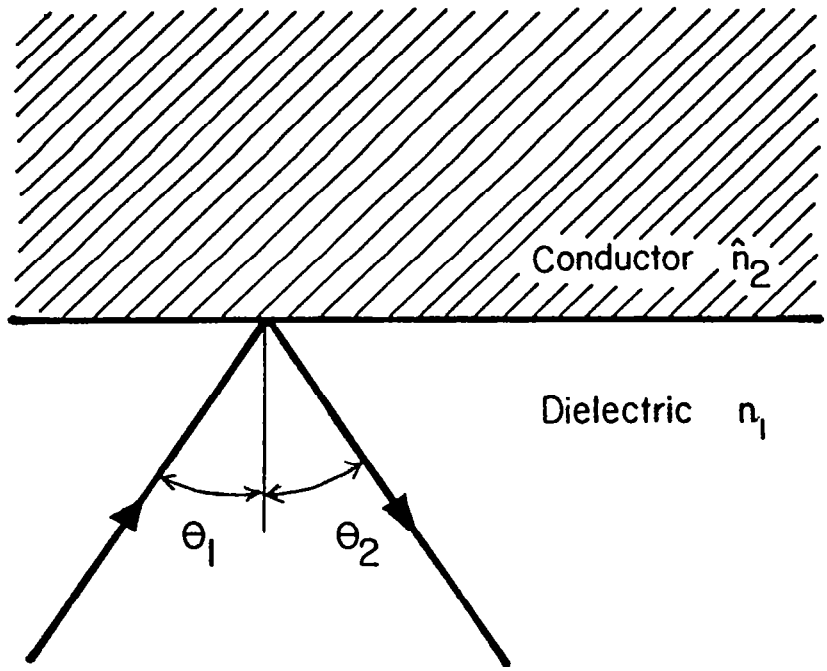

Figure 3.2 Dielectric Metal Interface

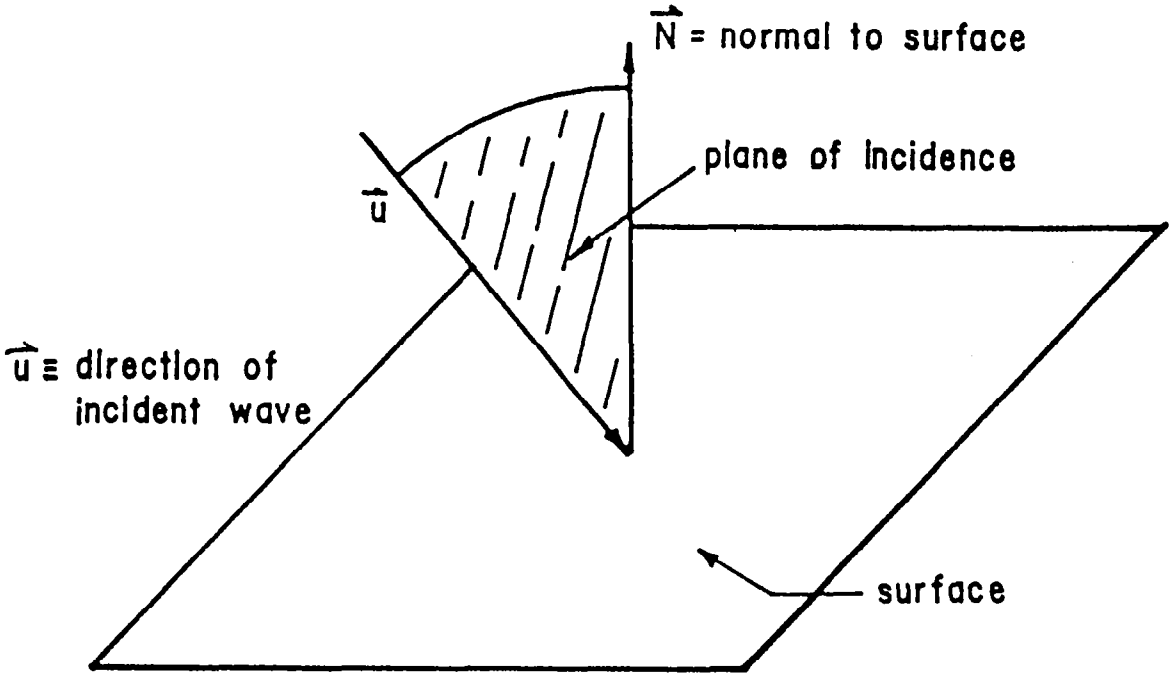

Figure 3.3 The Plane of Incidence

Therefore, we have the following equation for T.E. wave

$$r_{12} = \rho_{12} e^{i\varphi_{12}} = \frac{n_1 \cos\theta_1 - (u_2 + iv_2)}{n_1 \cos\theta_1 + (u_2 + iv_2)} .$$

The explicit expressions for the amplitude ρ_{12} and the phase change φ_{12} are obtained as:

$$\rho_{12}^2 = \frac{(n_1 \cos\theta_1 - u_2)^2 + v_2^2}{(n_1 \cos\theta_1 + u_2)^2 + v_2^2}$$

$$\tan\varphi_{12} = \frac{2v_2 n_1 \cos\theta_1}{u_2^2 + v_2^2 - n_1^2 \cos^2\theta_1}$$

For TM wave

$$r_{12} = \rho_{12} e^{i\varphi_{12}} = \frac{\hat{n}_2^2 \cos\theta_1 - n_1 \hat{n}_2 \cos\theta_2}{\hat{n}_2^2 \cos\theta_1 + n_1 \hat{n}_2 \cos\theta_2} .$$

After a straightforward calculation, we get

$$\rho_{12}^2 = \frac{[n_2^2(1 - \kappa_2^2)\cos\theta_1 - n_1 u_2]^2 + [2n_2^2 \kappa_2 \cos\theta_1 - n_1 v_2]^2}{[n_2^2(1 - \kappa_2^2)\cos\theta_1 - n_1 u_2]^2 + [2n_2^2 \kappa_2 \cos\theta_1 + n_1 v_2]^2}$$

$$\tan\varphi_{12} = 2n_1 n_2^2 \cos\theta_1 \frac{2\kappa_2 u_2 - (1 - \kappa_2^2)v_2}{n_2^4(1 + \kappa_2^2)^2 \cos^2\theta_1 - n_1^2(u_2^2 + v_2^2)} .$$

3.2.2 A Transparent Film on an Absorbing Substrate

In another case, consider reflection from a transparent film on an absorbing substrate (Figure 3.4). This is similar to what we encounter in our experiment with getting profiles from a metallic surface with a thin layer of oxide on the surface.

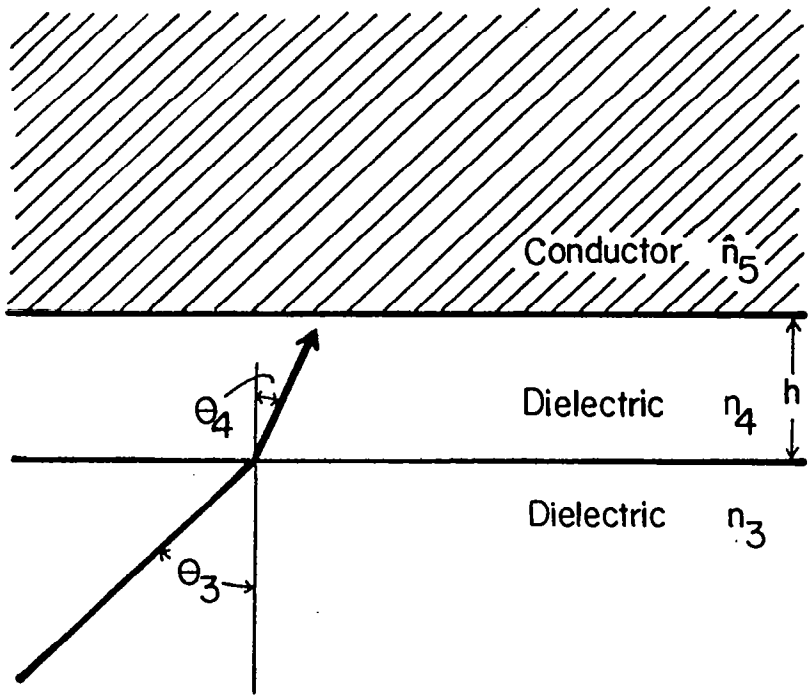

Figure 3.4 A Transparent Film on an Absorbing Substrate

In this case r_{34} is real while r_{45} is complex. The total amplitude ratio r is

$$r = \frac{r_{34} + \rho_{45} e^{i(\varphi_{45}+2\beta)}}{1 + r_{34}\rho_{45} e^{i(\varphi_{45}+2\beta)}}$$

After a series of calculations, we can obtain the phase change δ_r

$$\tan \delta_r = \frac{\rho_{45}(1 - r_{34}^2)\sin(\varphi_{45} + 2\beta)}{r_{34}(1 + \rho_{45}^2) + \rho_{45}(1 + r_{34}^2)\cos(\varphi_{45} + 2\beta)}$$

where ρ_{45} and φ_{45} have the same form as ρ_{12} and φ_{12} which can be found in the previous section; r_{34} is the amplitude reflectance when the radiation goes from air to the film and it can be easily calculated; and β takes into account the thickness of film h by the following expression:

$$\beta = \frac{2\pi}{\lambda_o} \hat{n}_4 h \cos \theta_4 .$$

It can be seen that the phase change with the film is distinctly different from the phase without the film. Therefore, in our interpretation of the profile which is basically a measurement of phase, we have to be cautious and take this into account. Also, the oxide may be partially absorbing which further complicates the analysis. Therefore, it is advisable that the complex index of refraction be determined.

3.3 Blok's Postulate

Blok's "flash temperature theory" is one of the most important concepts related to the interaction of counterformal surfaces [14,15,16]. The temperature at the surface, which is generated by frictional heat

between two surfaces is defined as

$$\theta_c = \theta_b + \theta_f$$

where θ_b is the bulk temperature and θ_f the maximum flash temperature. Blok proposed that this should be calculated as

$$\theta_f = \frac{1.11\ \mu W|U_1 + U_2|}{(K_1\rho_1C_1U_1 + K_2\rho_2C_2U_2)^{1/2}}\ (2a)^{-1/2}$$

where

$2a \equiv$ instantaneous width of the band-shaped contact area

$K_1, K_2 \equiv$ heat conductivity of the materials of bodies 1 and 2, respectively

$\rho_1, \rho_2 \equiv$ density of the materials of bodies 1 and 2

$C \equiv$ specific heat per unit mass

$\mu \equiv$ frictional coefficient between the surfaces

$W \equiv$ force acting on the surfaces

$U_1, U_2 \equiv$ velocities of the surfaces.

The group $\mu W(u_1 + u_2)$ denotes the amount of heat fed into the system and the other terms represent the ability of the system to receive and restore heat.

It is difficult to apply Blok's equation and use it practically because we need to assume μ. Blok [14,15] proposed the value 0.15 and Merritt [17] came up with an equation of the form

$$\mu \alpha [\eta^{0.15}(u_1 + u_2)^{0.15}(u_1 - u_2)^{0.5}]^{-1}[(r_1 + r_2)/(r_1 r_2)]^{1/2}$$

where η is the apparent area of contact, r_1 and r_2 are the radii of the two surfaces, respectively. He states that μ reaches a maximum static

value of about 0.15 for a steel-bronze combination and 0.2 for steel on steel. For cases of the counterformal bearing systems in which the materials are common to both interacting solids, θ_f can be reduced to the forms

$$\theta_f = 0.785\ \mu W(u_1^{1/2} - u_2^{1/2})/(K\rho Ca)^{1/2}$$

$$\theta_f = 0.62\ \mu W^{3/4}(u_1^{1/2} - u_2^{1/2})E^1/R^{1/4}K\rho C$$

$$\theta_f = 2.45\ \mu\rho_o^{3/2}(u_1^{1/2} - u_2^{1/2})R^{1/2}/(E^1)^{1/2}K\rho C\ .$$

It can be seen in the above expressions for θ_f that Blok's postulate only applies to straight mineral oils, i.e., those that do not contain extreme pressure additives.

3.4 The Mechanism of Scuffing

Scuffing is usually manifested in a number of ways. The machine would suddenly exhibit vibration and noise. There is also a progressive increase in operating temperature. Close examination of the surfaces would reveal an appearance like they had been welded together at various points. Sometimes there will be an abrupt increase in friction. A white etch-resistant phase [18] was also found after metallurgical examination of the scuffed surface. What is the cause of scuffing and how did it happen? There are various schools of thought as to the mechanism of scuffing, and the following includes some of the possible mechanisms.

3.4.1 Breakdown of Hydrodynamic Lubrication

It has been suggested by Cameron [19] that scuffing occurs as a result of the failing of the main hydrodynamic wedge mechanism. This

happens when the peripheral velocities of the components relative to their conjunctions are equal and opposite. Hydrodynamic action then depends on the much weaker viscosity wedge mechanism, resulting from the difference in temperature between the surfaces approaching and leaving the contact. However, this weaker mechanism may not be able to give the necessary hydrodynamic support.

3.4.2 Breakdown of Boundary Lubrication

Cameron [20] brought in the explanation of the boundary lubrication breakdown in terms of the thickness of the film. He suggested that "a thick film is better than a thin one." As the film gets thinner relative to the roughness, there is longer contact between each asperity and more time for any surface film to desorb; hence the lower temperature needed for the residence time to equal the local asperity contact time. The opposite situation will arise for a thicker film.

Dyson [2] based on findings from Bowden and Tabor [21] that many systems showed a well-defined rise in the coefficient of friction as the bulk temperature was increased, and suggested the total contact temperature was identical with the bulk temperature. He compared the bulk temperature with the temperature for the breakdown of boundary lubrication in an attempt to explain scuffing. However, this theory only works in a few cases and is not generally accepted.

3.5 The Influence of Surface Films on Scuffing

The theories on scuffing discussed thus far concern mostly the physical aspects. But scuffing is known to be quite sensitive to chemical and metallurgical factors. The idea of the formation of protective film

so that scuffing can be avoided is quite welcomed by lubrication engineers. The extreme pressure additives, which contain sulfur, chlorine, and phosphorus, serve this purpose. The interaction between these additives is quite complicated and not well understood. For instance, Godfrey [22] suggested that a phosphate was formed when steel sliding on steel was lubricated with tricresyl phosphate. On the other hand, Shafrin [23] used Auger spectrophotometry and found that exposure to TCP initially formed a phosphide on a steel surface but that this phosphide changed to a phosphate on prolonged exposure.

PART 4

APPARATUS

There are two main apparatuses used in the experiments: the Phase-Locked Interference Microscope (P.L.I.M.) and the Ball/Plate Bearing Contact. The P.L.I.M. was constructed based on a design by Johnson, Leiner and Moore [25] at the Institute of Optics of the University of Rochester. The Ball/Plate Bearing Contact was constructed originally by Mr. Frank Choi [26] and was modified to accommodate our samples. The following is a description of the two systems.

4.1 Phase-Locked Interference Microscope

There are two subsystems in the P.L.I.M.: the optical system and the electrical system. Together they form a closed loop configuration and allow the profiling of surfaces at a high degree of resolution without any physical contact.

4.1.1 The Optical System

Basically, the instrument is a Twyman-Green interferometer. Together with the alternating current electronics, it is capable of a phase resolution of 1/200 of the wavelength of the radiation (e.g., ± 30 Å in the case of the red He/Ne laser line - 6328 Å). Figure 4.1 is a schematic drawing of the instrument's optics. The instrument can be operated with either a He/Ne laser or an Argon Ion laser with four lines at 5145 Å, 4880 Å, 4765 Å and 4579 Å.

Radiation from the laser is expanded and cleaned by a beam expander which consists of two positive lens, with 10 mm and 80 mm in

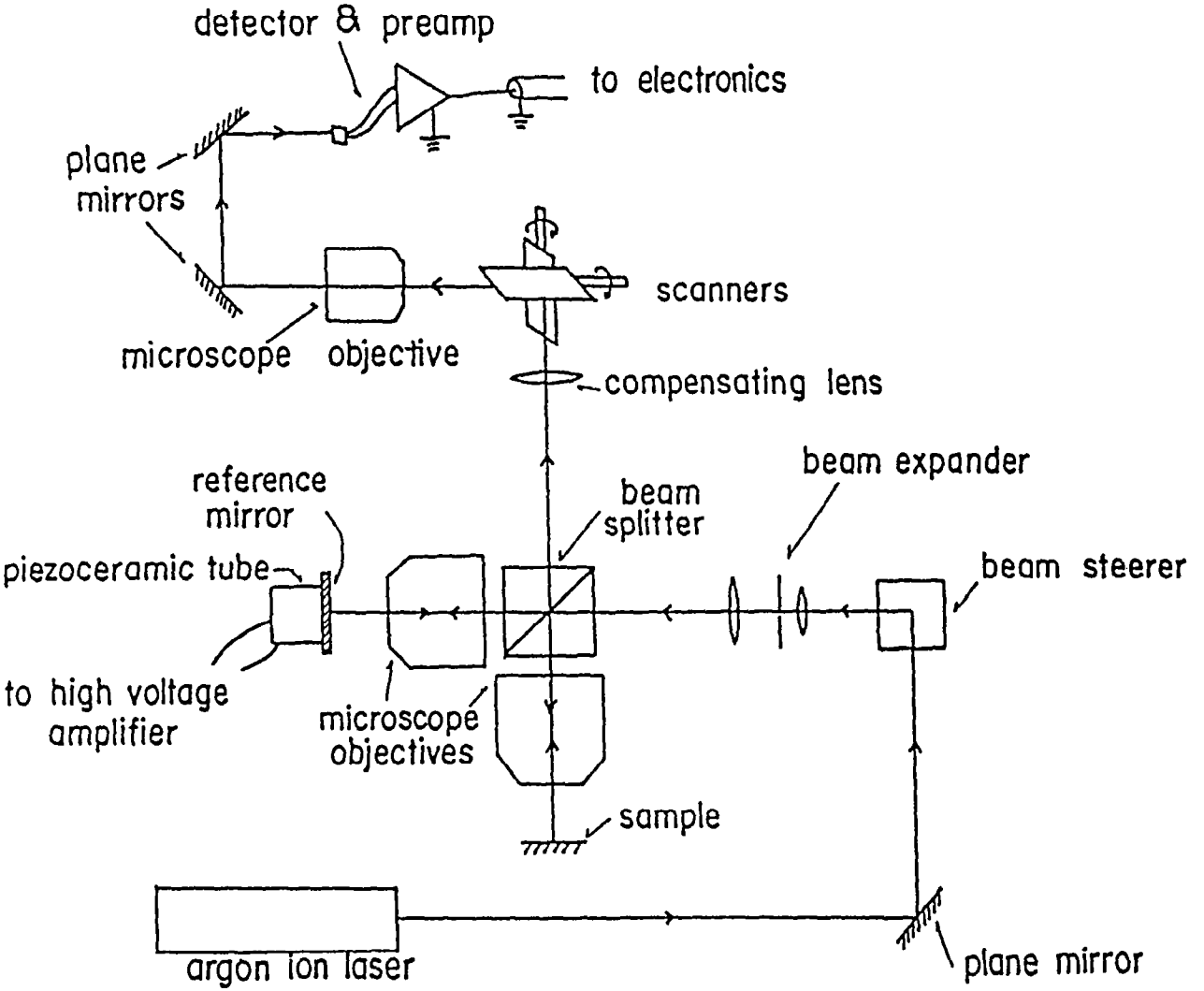

Figure 4.1 Schematic Drawing of Interferometer

focal length. The spatial filter in between has a pin-hole of 0.2 mm. Then the light is split by a beamsplitter; part of the radiation continues to a flat reference mirror oscillated by a piezoceramic transducer and part is deflected to the sample surface by way of a microscope objective. The split beams are reflected back to the beamsplitter, recombined, expanded by a microscope objective, and ultimately transferred to a photodiode. A compensating lens (f = + 60 mm) images the image formed by the microscope objectives to the objective near the detector. Two scanning mirrors can be turned in a way as to make possible scans parallel to the x- and y-directions in the same plane. The x-mirror scans horizontally and the y-mirror increments in small steps vertically. Phase differences between the two beam paths generate fringes in the detector plane. As the surface is scanned in the x-direction, the phase difference between the interferometer beams is changed and the fringes are moved over the detector surface proportionally, as determined by the optics.

4.1.1.1 Calibration of Phase and Horizontal Distance

At the present stage of the instrument, scanning is done nonlinearly, by varying the angle of the recombined beam with respect to the optic axis of the microscope objective facing the sample. For small excursion of the scanning mirror, the departure of a scan from linearity is small. The surface profile of Figure 4.2, obtained with an inexpensive reflection-type diffraction grating, is an example. The distance between the first and second peak is about 10% greater than that between the second and the third peaks. The intensity of the peaks of Figure 4.2

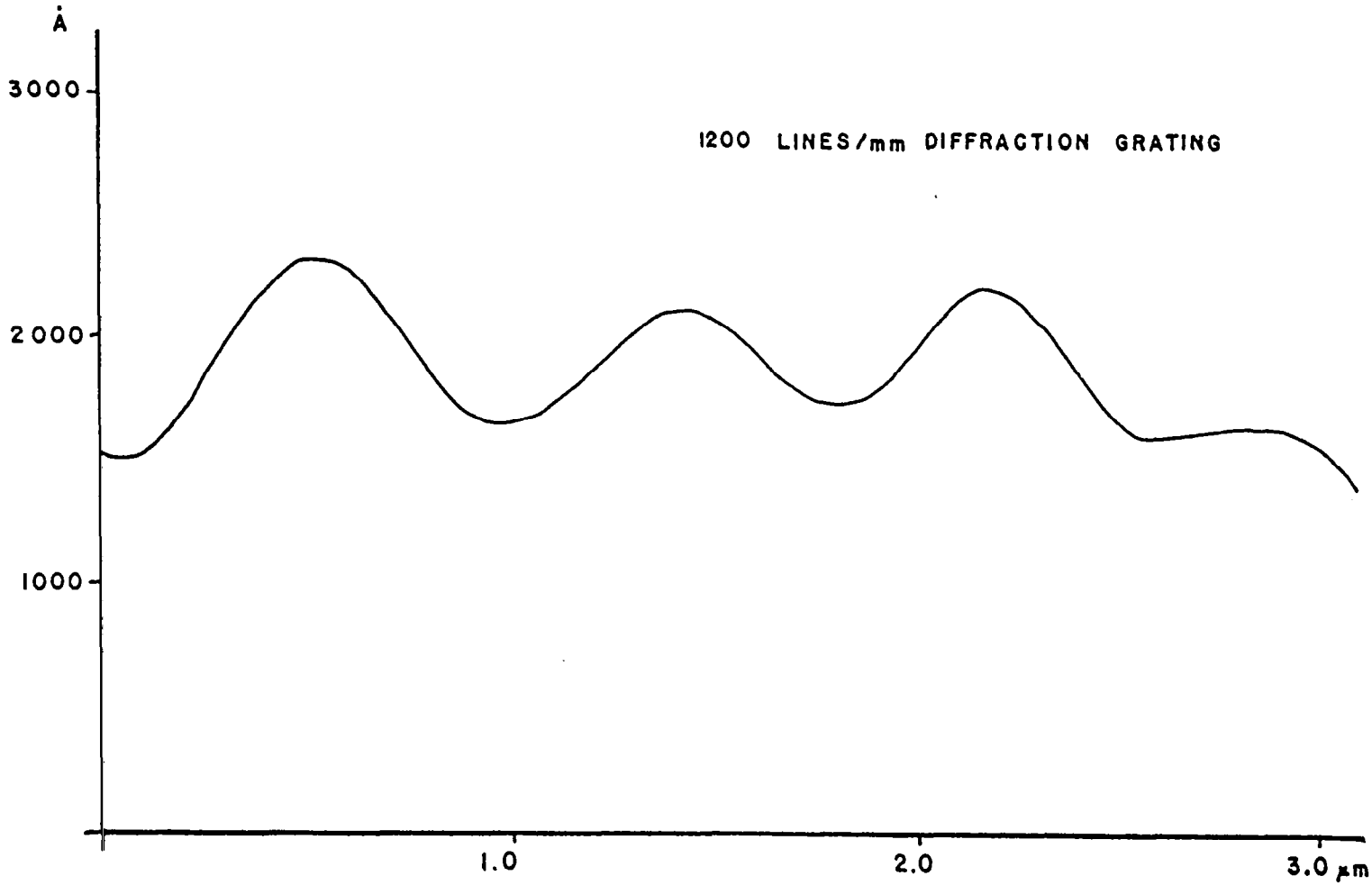

Figure 4.2 Profile of a 1200 lines/mm Diffraction Grating

is seen to fall off toward the right. The reason is the lack of planarity of the objective lens when used off-axis. Beyond a distance of 2.5 μm from an arbitrary chosen position, the scanning optics are evidently out of the field of view. The intensity of the peak at 3.0 μm is much less than that of the other peaks. As the grating was blazed, the slope to the left of every peak is expected to be shorter and steeper than the slope to the right. The angles are also about correct. The reason for the gentleness of the peaks and valleys, where sharp corners are expected, is the horizontal limit of the objective lens in conjunction with the interferometer optics.

Distance calibration of the instrument is simple. In the horizontal plane, the distance of successive peaks of a reflection grating provide the required information (Figure 4.2). Depth calibration is done very accurately by the phase jump in the detector plane. The separation between two successive interference fringes corresponds to a phase difference of 2π between the sample and the reference beams. In air, because of the phase reversal on reflection by the sample surface, this separation of fringes corresponds to a change in apparent depth of sample surface profile of half a wavelength of the laser light. The phase jump values for the different wavelengths are listed in Table 4.1.

For instance, in the case of the He/Ne laser with a wavelength of 6328 Å, half of the wavelength or 3164 Å corresponds to a phase jump of 10 V for the electric recorder output potential. Any voltage changes are directly proportional to the phase changes and, therefore, to the changes of depth and the conversion can be carried out in terms of the 316.4 Å/volt relation.

4.1.1.2 Microscope Objectives Used

When the system was initially set up for single wavelength operation with the He/Ne laser, two pairs of refracting microscope objectives (10 × and 40 ×) were used. Most of the profiles were taken with the 40 × objectives and this introduced experimental error, besides being cumbersome. The error was introduced during the acid treatment in which a drop of acid was applied onto the surface after a surface profile had been taken. Because of the short working distance of the 40 × objective, one may accidentally hit the sample in the process and knock the sample out of place. Consequently, the profile taken after the acid treatment would be of a different spot which may be adjacent to the profile taken before the treatment. Furthermore, the acid may splash onto the objective and cause the metallic parts to corrode.

Therefore, we tried a pair of Ealing Cassegrainian reflecting objectives (Figure 4.3) which have a working distance of 8.0 mm. However, they did not produce images that are satisfactory in quality. After researching the theory of these lenses, we found that they may not be suitable for this work because a portion of the paraxial beam is cut off and this reduces the contrast of the image. Figure 4.4 shows how the modulation transfer function is affected when various percentage of the beam is obstructed [27]. The decrease in the function values for the low spatial frequencies may make the lens unsuitable for our use. This is because most bearing surfaces are quite rough and this translates to low spatial frequencies.

Nonetheless, we tried another new pair of Zeiss Jena objectives and this results in significant improvement for the system. The new

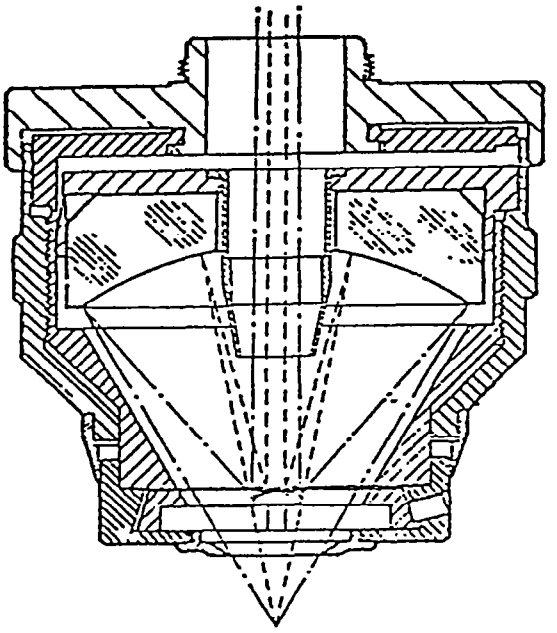

Figure 4.3 Cross-sectional View of Ealing Reflecting Microscope Objective

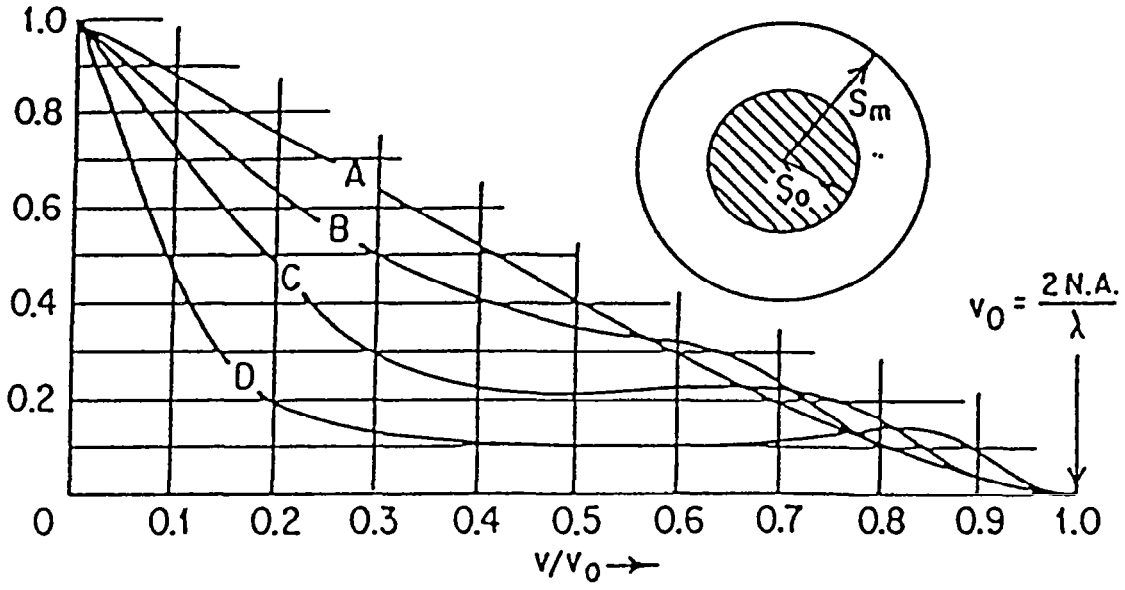

A) $s_0/s_m = 0.0$
B) $s_0/s_m = 0.25$
C) $s_0/s_m = 0.5$
D) $s_0/s_m = 0.75$

Figure 4.4 The Effect of a Central Obstruction on the Modulation Transfer Function of an Aberration Free System.
A) $S_o/S_m = 0.0$, B) $S_o/S_m = 0.25$, C) $S_o/S_m = 0.5$,
D) $S_o/S_m = 0.75$

objectives are both reflecting and refracting (Figure 4.5). Even though a portion of the central beam is blocked off, they worked beautifully despite previous experiences. This is presumably due to: (i) the two objectives are precisely matched in the factory, and (ii) the blocked center portion is very small compared to the two-inch diameter Cassegrarian collecting mirror. This has an even longer working distance of 17 mm and it also brings about a number of advantages and they are:

- Longer working distance, allowing easy application of acid treatment and can view through window.
- Has a cover glass for protection against any splashing of acid into the optics.
- Apochromatic optics - allows the operation of multiple wavelengths with the least amount of chromatic abberations.

However, these objectives have a metric thread of M20 × 0.8 (diameter × pitch) and require a special adapter.

The specifications of all the objectives are listed in Table 4.2 for comparison purposes.

4.1.1.3 Special Sample Holders

Two special holders were constructed for samples that cannot be mounted in the normal holder. One is for fuel tubes and the other one is for 2 1/4" bearing balls. Both are made such that they can be mounted to four parallel rods in a square type of configuration with a center-to-center distance of 3 in. for one side of the square.

The bearing holder was constructed in a way that the bearing can be centered. The 2 1/4" bearing ball sits in a cup which is mounted

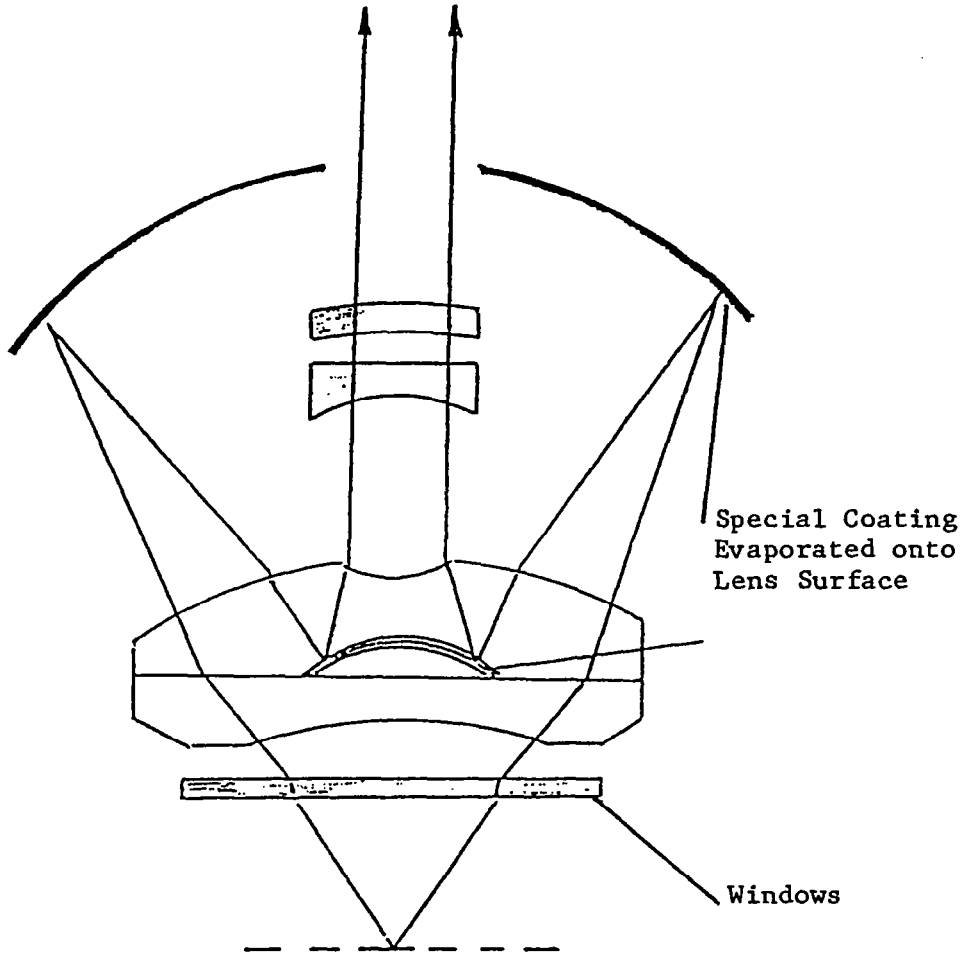

Figure 4.5 Cross-sectional View of Zeiss Jena Objective

TABLE 4.2

SPECIFICATIONS OF THE DIFFERENT MICROSCOPE OBJECTIVES

Numerical Aperture: NA = n sin I; I = the Half Angle of the Cone of Light Entering the Objective; n = the Index of Refraction of the Medium Between the Object and the Lens

Optics	Magnification	Make	Numerical Aperture	Working Distance (mm)	Field of View Diameter (mm)
Refracting	10 ×	Swift	.25	6.8	1.8
	40 ×	Swift	.65	.50	.45
Reflecting	36 ×	Ealing	.50	8.0	.50
Reflecting and Refracting	40 X	Zeiss Jena	.50	Full - 18.7 with cover glass - 17.0	.7*

* As measured in our laboratory.

in an oversized hole. The lateral position of the cup can be adjusted by means of turning three screws which dictates the cup position.

The second holder is for fuel tube samples. A linear slider, which has a precision of one-hundreth of a millimeter or better, is mounted onto an aluminum plate. The fuel tube is clamped down onto a V-groove fixture which can be slid back and forth. The holder should be mounted with the rotating wheel close to the user and the step of the fuel tube up against the edge of the groove. This will allow the maximum length of tube to be examined and ensures repeatability. To align the stage so that the laser spot hits the very top of the cylindrical tube, the user can adjust the four screws which decide the position of the slider.

4.1.2 The Electronic System

In conventional interference microscopy, only an accuracy of $\lambda/20$ is possible with visual determinations of phase. However, with the electronic system the P.L.I.M. can produce profiles which have an accuracy up to $\lambda/200$. The following is a description of the phase-locked electronics and how the entire system operates.

4.1.2.1 Phase-Locked Electronics

The purpose of the Phase-Locked Electronics is to generate a signal proportional to the phase difference of two interfering wavefronts; namely, one from the reference mirror and one from the sample, for a given point in the field. Since the interfering wavefronts or the fringe pattern is essentially a topographical map, this slow-varying phase signal when scanned in one direction along a fringe is the sample

surface profile, assuming the reference mirror is perfectly flat and there is no oxide layer on the sample. The block diagram in Figure 4.6 illustrates the major components of the system.

In order to measure the phase properly, the interference fringes should have an intensity maxima that is resolvable by the detector. The fringe pattern is being modulated by way of a piezo-ceramic crystal, on which the reference mirrir is attached, at a frequency of 20 kHz. The amplitude of modulation should not exceed 1/4 λ. When all the above conditions are fulfilled, the photodiode should detect a signal primarily consisting of 20 kHz and/or 40 kHz. There are two possible situations: (i) a bright fringe falls onto the detector, (ii) the detector does not see a bright fringe (either falls between the fringes or sees a dark fringe). Since the 40 kHz is the first harmonic of the 20 kHz signal, and the two signals are either in phase or π out of phase. If we filter out the 20 kHz signal, sample the signal at the crest and the trough of the sinusoidal signal, and then take the difference between the two samples signals, we can determine the amplitude of this 20 kHz signal. In the case of (i), the amplitude of the 20 kHz signal should be almost zero. This is because the detector sees the variation in intensity from one side of the side to the other. On the other hand, when the detector does not see a bright fringe as in the case of (ii), the output of the difference amplifier will get a signal; though not linearly, proportional to the voltage it needs to cause the piezoceramic crystal to move the fringe to the detector. This is referred to as an error signal and is applied to an integrating stage. The output

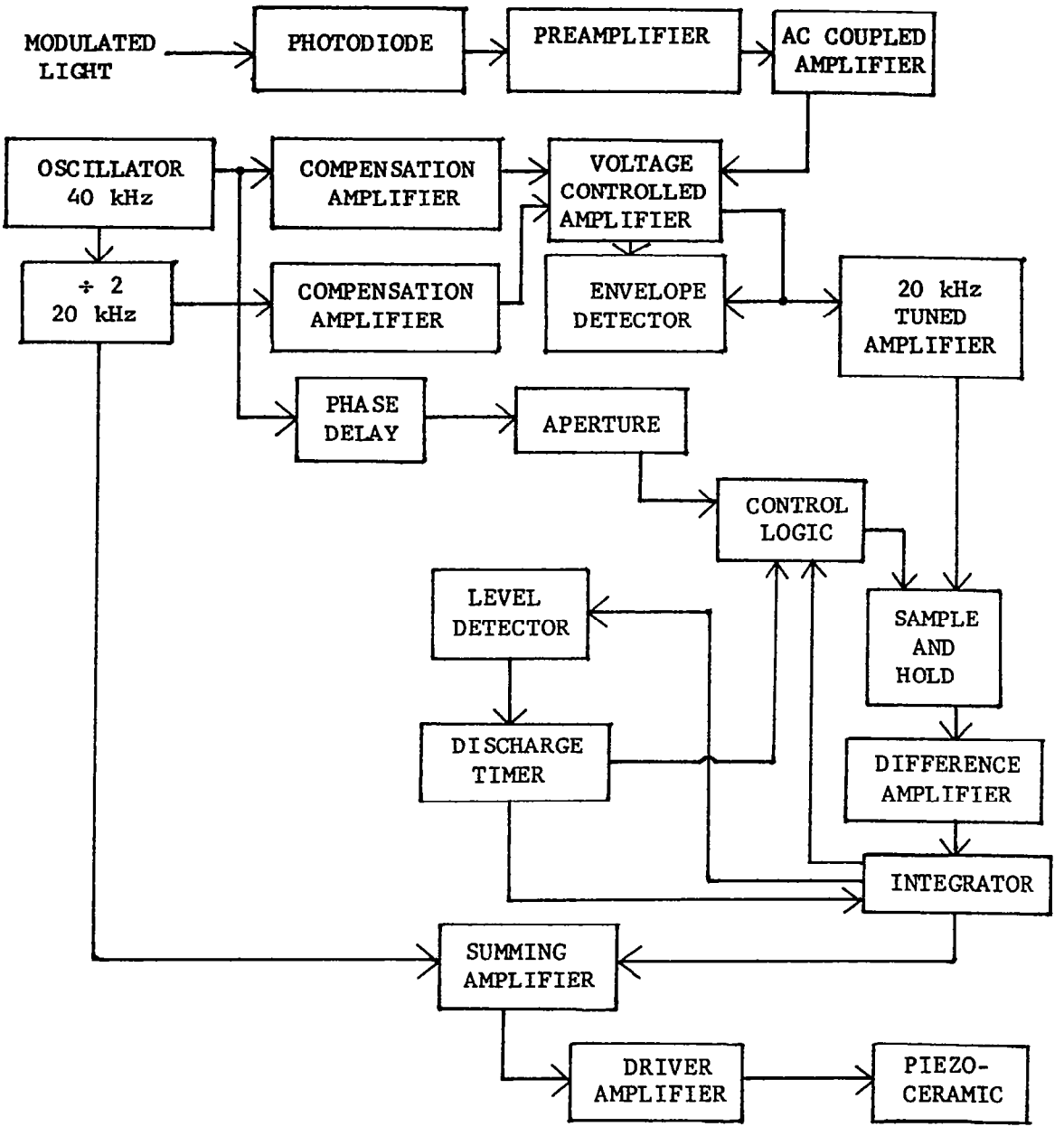

Figure 4.6 Block Diagram of Phase-Locked Electronics

of the integrator is summed with the modulating signal as the slow-varying signal and then sent to the piezoceramic crystal driver. As a result, the system becomes a null-seeking function.

Since the bright fringe can be moved to the detector and remains there as long as the error signal is applied, the system is considered locked on the fringe and that is why it is called "phase locked."

With the X-galvanometer that moves the fringe across the detector, a nonzero error signal is then continuously generated. This signal is directly proportional to changes in the phase difference between the two interfering wavefronts, or this is the surface profile of the sample.

Since the integrator has a limited range, the system is designed such that the integrating capacitor would discharge the voltage for a set length of time. This will release the fringe and the system will try to lock onto a new fringe as soon as the discharge is over. The discharge is referred to as the phase jump and it is utilized in the phase calibration of the system. When this is properly set, one phase jump corresponds to one fringe or half the wavelength used.

4.1.2.2 System Operation

At the present, the system is constructed for stand-alone operation (Figure 4.7). The outputs are connected to both an X-Y recorder and a storage oscilloscope. Distance versus phase can be obtained or plotted on paper. The X-scan signal is amplified and can be biased so that it can be accommodated by the storage oscilloscope. The schematic

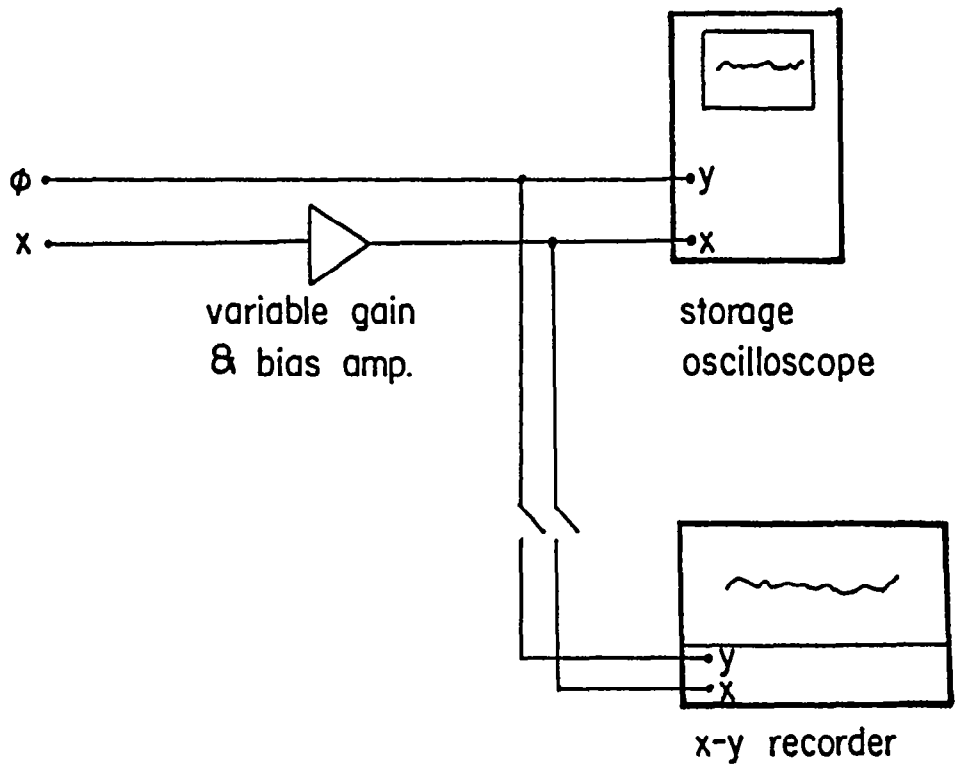

Figure 4.7 Output System of P.L.I.M.

for this two-stage amplifier is shown in Figure 4.8. Further, the signal to the X-Y recorder can be isolated by opening two switches. This is implemented so that the abrupt phase jump signals cannot damage the recorder.

Most often one profile alone is not enough to supply enough information about the surface. The Y-bias control on the front panel allows the user to adjust the Y-mirror slightly after the X-mirror has made a scan. A series of profiles which are along side of each other can be obtained in this manner manually.

4.2 Ball/Plate Bearing Contact

There are two different setups which allow us to prepare samples for microscopic examinations. They were ball/plate bearing EHD contacts in which a bearing ball of 2.25 in. diameter was rotated by a horizontal shaft either on top of a diamond window (the plate) [26], in the bottom of a cup containing the test fluid, or underneath a sapphire window (the plate) [28]. In either case, the ball was loaded from the top. The former setup was used primarily as part of the infrared analysis work done in the same laboratory where the author worked. Some of the samples run in Polyphenyl Ether were operated in the above setup. The second setup, from which more samples were prepared, was originally designed for EHD film thickness and traction measurements. The contact obtained the lubricant by a wetting and dragging mechanism. Therefore, conditions were such that starvation was excluded in both cases.

Since the former setups were described in detail previously, the reader should consult the references for more information. However,

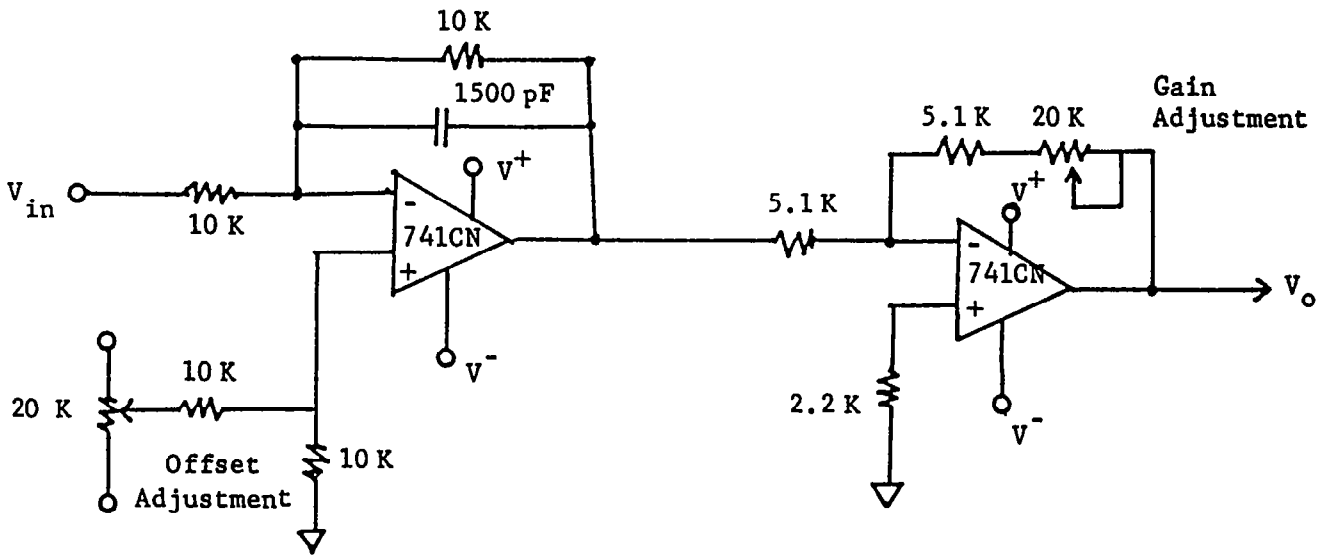

Figure 4.8 Schematic of Two-Stage Amplifier

there had been some modifications to the latter setup. The following is a description of the modifications.

4.2.1 Modifications of the Ball/Plate Bearing Contact

The setup was modified so that we could substitute the sapphire windows with M-50 steel samples and ran the plates against the ball for different periods of time. In order to keep the experiment controlled, the same bearing steel was chosen to run against each other. Only 13/16 in. diameter balls were available to us at the time and they were significantly smaller than what the setup was designed for. A new shaft was machined so that the balls could be held in place. A holder was designed to hold the samples and it was mounted in the location where the sapphire window used to be. The position of the alignment bearings was also raised to accommodate the smaller size ball. Figure 4.9 is a schematic drawing of the setup. The tubing which is used with the varistaltic pump caused some problems. With the 1/8 in. inner diameter Tygon tubing which is ideal for the setup, problems arise because the tubing would crack in about an hour's operation. We eventually had to go to the 1/4" ID tubing, which seemed to have reduced the problem. However, the user should be aware of this problem when operating the setup.

Other modification or improvement was the connecting of the strain-gage readout to a strip-chart recorder. This allows dynamic measurements of friction or traction. Since the signal from the strain gage indicator was too large for one scale and too small for another, the output was connected to a voltage divider and the signal was reduced in half before the strip-chart recorder took it in.

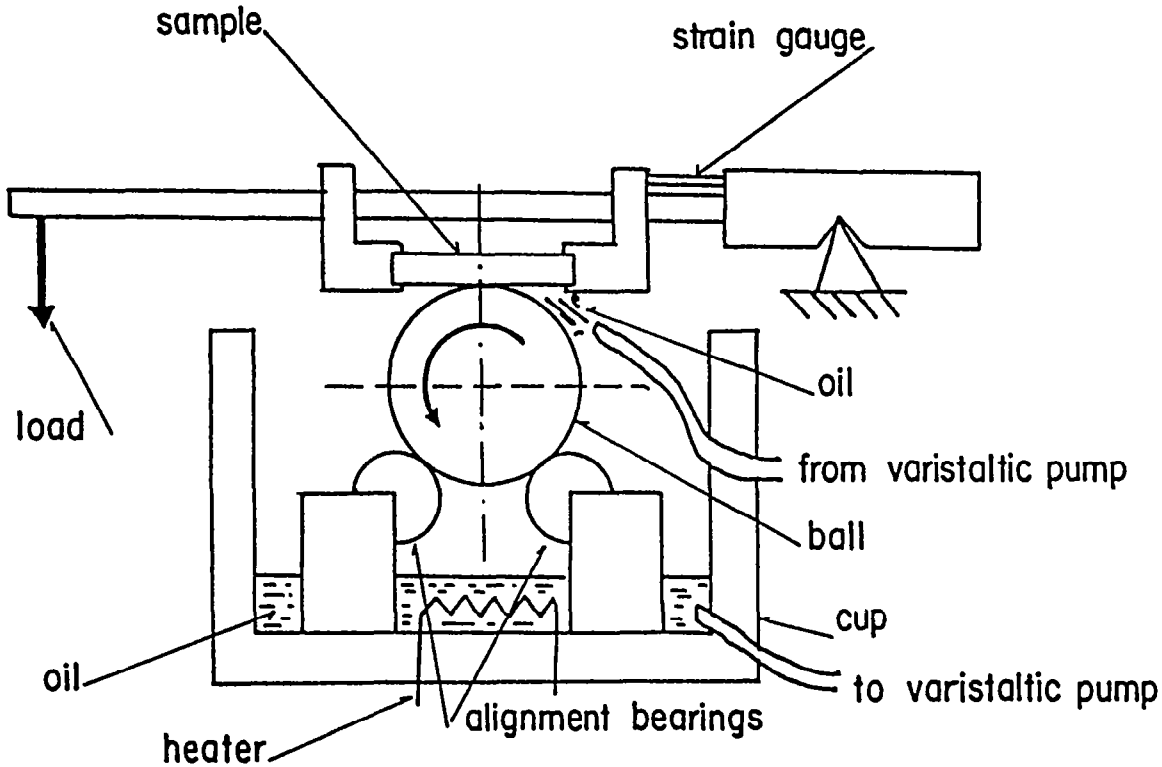

Figure 4.9 Schematic of Ball/Plate Bearing Contact

PART 5

MATERIALS

There were basically two sets of experiments carried out during the course of this research work. Each set utilized different bearing materials and lubricants, and the concentration of the probe solution was also different. The first set of experiments was the study of the reactivity of the scuff mark versus outside of the scuff mark, as well as the reactivity of the reference plate after being subjected to different temperatures. The second set of experiments was the study of the topological reaction rate of the M-50 bearing steel in lubricants of various additives.

5.1 Materials Used in the First Set of Experiments

5.1.1 Bearing Materials

The bearing balls were of 2.25 in. diameter and made of 440 C stainless steel. Some of them were coated with titanium nitride by chemical vapor deposition (CVD method) to a uniform thickness of about 4 μm, as described by Hinterman and Boving [29]. The smoothness of all the ball surfaces was about 0.01 μm initially (mean peak height), as determined with our optical profilometer. Since the lubricant film thickness in the EHD contact under the heaviest load and at the smallest continuously maintained shear rate was at least 0.5 μm as determined earlier [29], direct asperities interaction could only occur when the sliding speed was gradually reduced to zero.

5.1.2 Lubricant

The balls were run with polyphenyl ether fluid (5P4E) either pure or containing 1% by volume of 1,1,2-trichloroethane. Both of these fluids were also referred to in the same earlier publication [28].

Before use in the experiments discussed below, the balls were cleaned with acetone and mounted in a holder specially constructed for the interference microscope.

5.1.3 Stainless Steel Reference Plates

The stainless steel reference plates were of smoothness similar to that of the balls. They were made of polished No.304 stainless steel and were 1" × 1" × 1/16" in size.

5.1.4 Probe Solution

The probe solution was 0.04 M hydrochloric acid in absolute ethyl alcohol. It was titrated against a potassium chloride solution for accuracy.

5.2 Materials Used in the Second Set of Experiments

5.2.1 M-50 Bearing Steel

The M-50 is a 4%, Cr, 4% Mo, 1% C, martensitic steel. The heat treatment procedure was the following:

Preheat	816°C
Harden	1110°C
Quench (in molten salt)	552°C
Air cool	Room temperature

Temper* (2 hours)	538°C
Air cool	Room temperature
Temper (2 hours	538°C
Air cool	Room temperature
Three more tempers at	524°C

* Tempering should be started as soon as room temperature is reached to avoid cracking.

Our samples were heat treated by a local heat-treating company. The hardness of the steel after the heat treatment was 62-63 (Rockwell C).

Our samples (20.6 mm diameter balls and 22 mm × 11 mm × 7 mm plates) were ground before the heat treatment. After heat treatment a grayish finish appeared on the surface. The plates were then mounted in epoxy plastic and all the specimens were lapped by machine. They were polished successively with 240, 400 and 600 grade sandpaper under water, then with 9 micrometer diamond-imbedded paper without water, and then with 0.3 micrometer aluminum oxide under water, until practically a mirror finish was reached. Under the metallurgical microscope (nital etching) the structures typical of tempered martensite were apparent (Figures 5.1a and b). Some chunks of carbide (white areas) can be seen.

The steelmaker also supplied us with the following physical properties for this steel:

Specific gravity	8.0
Specific heat, J/kgK	418.6
Thermal conductivity, watt/cm °C	
at 100°C	0.37
300°C	0.35
500°C	0.34

Figure 5.1a Photomicrograph of M-50 Steel as Used. The surface was etched with nital. Magnification 500 ×

Figure 5.1b Photomicrograph of M-50 Steel as Used. The surface was etched with nital. Magnification 1600 ×.

5.2.2 Lubricant

The lubricant used in this work was the base oil of a research lubricant prepared by NASA and designated as G-MIL-99. The fully formulated lubricant was designed to represent those manufactured under MIL-L-23699 specification.

Specifically the base stock of G-MIL-99 is pure trimethylol propane triheptanoate (TMPTH), which has the following structure:

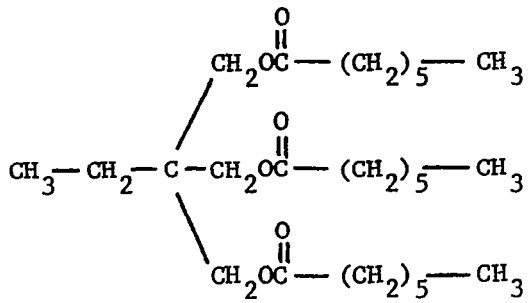

Its principal physical properties are:

Viscosity, cs at 98.9°C	3.5
at 37.8°C	15.2
Pour point, °C	67.8
Specific gravity, 25°C	0.963

Shell 4-ball wear test

Force	Scar Diameter
Newton	mm, at 54°C 600 rpm, 1 hour
9.8	0.21
98	0.43
392	0.57

Besides the base oil TMPTH, a number of lubricants containing different additives from the fully formulated lubricant were also used. They are described as follows and more information can be found in Appendix D.

1) 0.0209% benzotriazole (BTZ), a corrosion inhibitor, in trimethyolpropane
2) 1.047% dioctyldiphenylamine (DODPA), an antioxidant, in TMPTH
3) 1.047% phenyl-alpha-naphthylamine (PANA), an antioxidant, in TMPTH
4) 2.618% tricresyl phosphate (TCP), an antiwear additive, in TMPTH
5) Generic MIL-L-23699 (G-MIL-99) or the fully-formulated oil, with 2.5% TCP, 1% DODPA, 1% PANA, 0.02% BTZ and the rest is TMPTH.

5.2.3 Probe Solution

The concentration of the probe solution was 0.011 M hydrochloric acid in absolute ethyl alcohol and the concentration was also verified.

PART 6

EXPERIMENTAL PROCEDURES AND RESULTS

As described in Part 5, there were basically two sets of separate, yet related experiments. The first set of experiments was a study of the microscopic contour changes as a result of the acid treatment. Based on the contour changes, the second set was a measure of the topological reaction rate as a function of operating time.

6.1 Measurement of Microscopic Contour Changes

6.1.1 Preparation of the Ball Samples

The balls were taken from the rigs after many hours of operation on polyphenylether with and without 1% of 1,1,2-trichloroethane. The steel balls without titanium nitride would have failed by scuffing.

The balls were cleaned with acetone, soaked in absolute alcohol overnight, rinsed, and placed in a vacuum desiccator to remove the absorbed alcohol. The principal purpose of applying the vacuum was to avoid the destruction of the filament in the scanning electron microscope.

6.1.2 Examinations of Ball Surfaces Run in Polyphenyl Ether with the P.L.I.M.

Since the score or scuff marks on the balls were typically 100 μm in diameter, we found it useful to work with two different refracting microscope objectives, 10 × and 40 ×, the former enabling us to overlap the mark and the latter to look inside of it. Still higher magnification could have given us better lateral resolution but the short working distance would have made the application of the test fluid

(0.04 M alcoholic hydrochloric acid) very difficult. Consequently, the installation of the reflecting microscope objectives with a longer working distance made our work very much easier.

Figure 6.1 shows two of an area of such a used steel bearing ball, which includes parts within and without the scuff mark. A drop (0.05 mℓ) of test fluid was applied from a measuring syringe, care being taken not to move the ball-microscope alignment in any way. For this work, the ball was rigidly mounted on a holder, which itself was rigidly attached to the microscope frame, so that the entire system would vibrate as one unit. The drop would evaporate rapidly, and then another profile was recorded. As can be seen from Figure 6.1 the changes outside the scuff mark were much smaller than the changes inside the scuff mark and, in either case, most of the profile was lowered by the test reaction.

In another instance, the difference of reaction inside and outside the scuff mark was even more drastic. Figure 6.2 presents a clear indication that changes of profiles can be both upwards and downwards. There can be no doubt that the changes produced by the test probe within the scuff mark were much greater.

Figure 6.3 represents the effects outside of the scuff mark of two successive probes on stainless steel bearing ball run to scuffing on polyphenyl ether. The reactivity was much greater for the second treatment than for the first. The first treatment might have attacked the oxide layer, the second the metal itself.

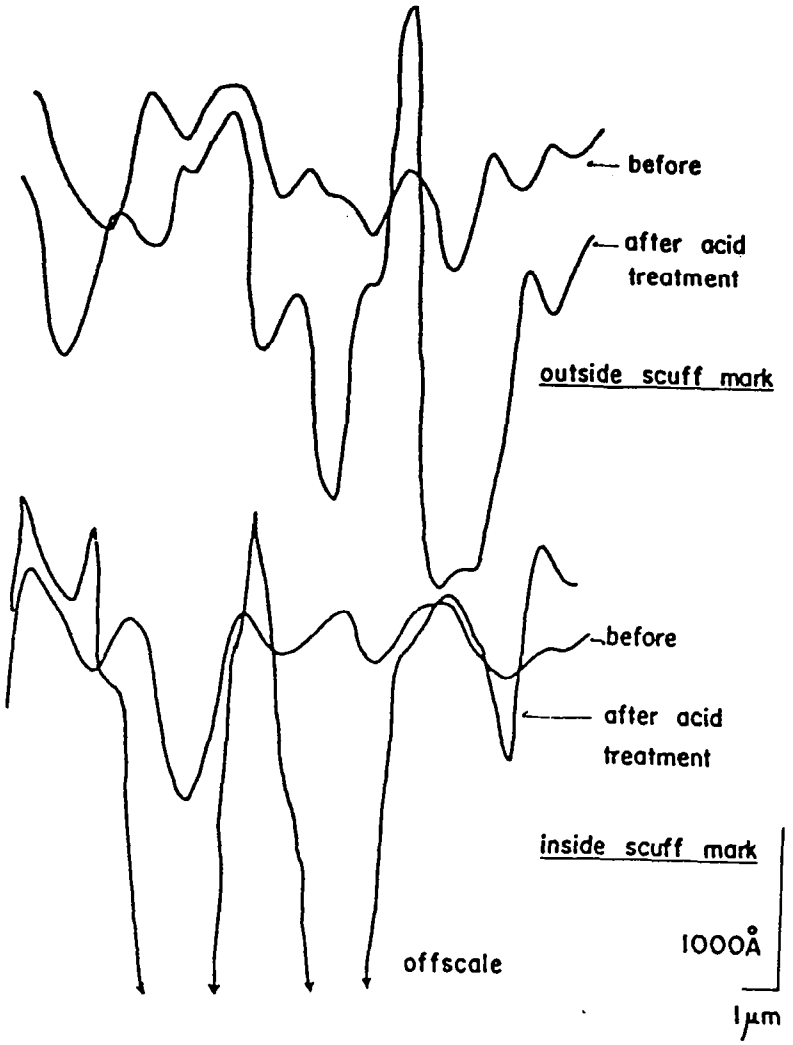

Figure 6.1 Surface Profiles of a Stainless Steel Bearing Ball Scuffed in Polyphenyl Ether, Before and After a Test Probe of 0.04 M Alcoholic Hydrochloric Acid was Applied. The top traces were taken outside the scuff mark and the bottom traces were taken inside the scuff mark. (in order to avoid overlap, the traces taken after the acid treatment were set off.)

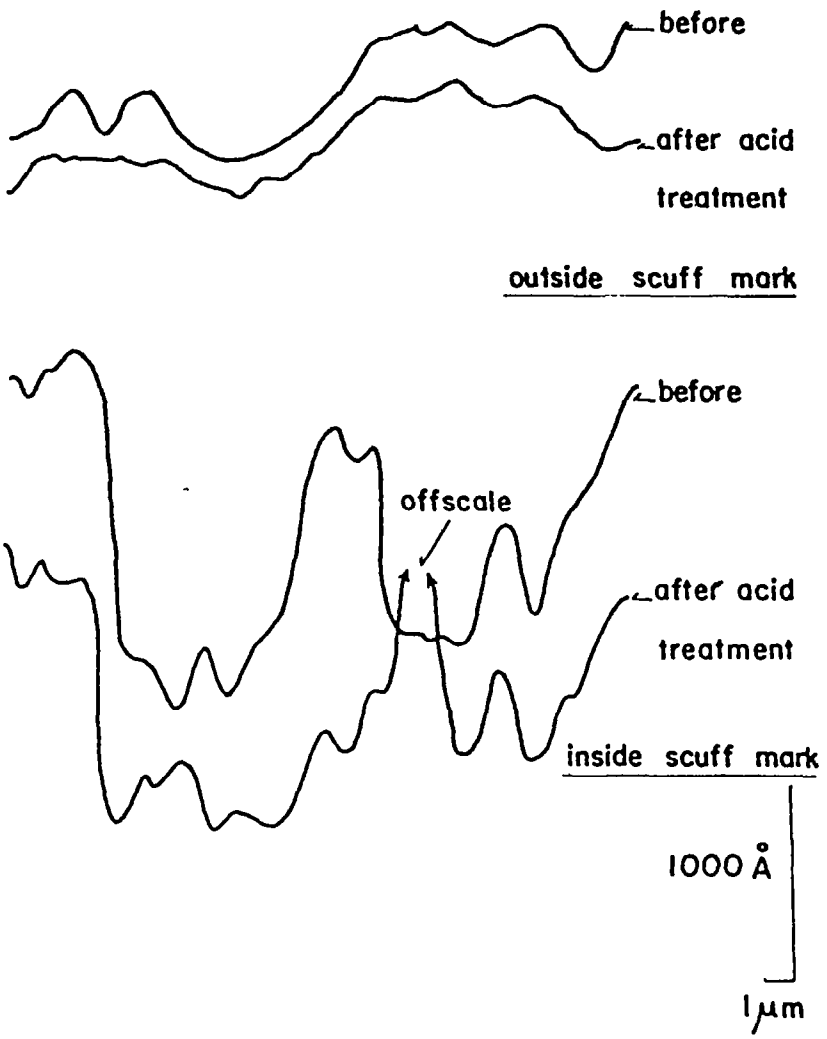

Figure 6.2 Surface Profiles of Another Stainless Steel Bearing Ball Scuffed in Polyphenyl Ether, Before and After a Test Probe of 0.04 M Alcoholic Hydrochloric Acid was Applied. The top traces were taken inside the scuff mark. (In order to avoid overlap, the traces taken after the acid treatment were set off.)

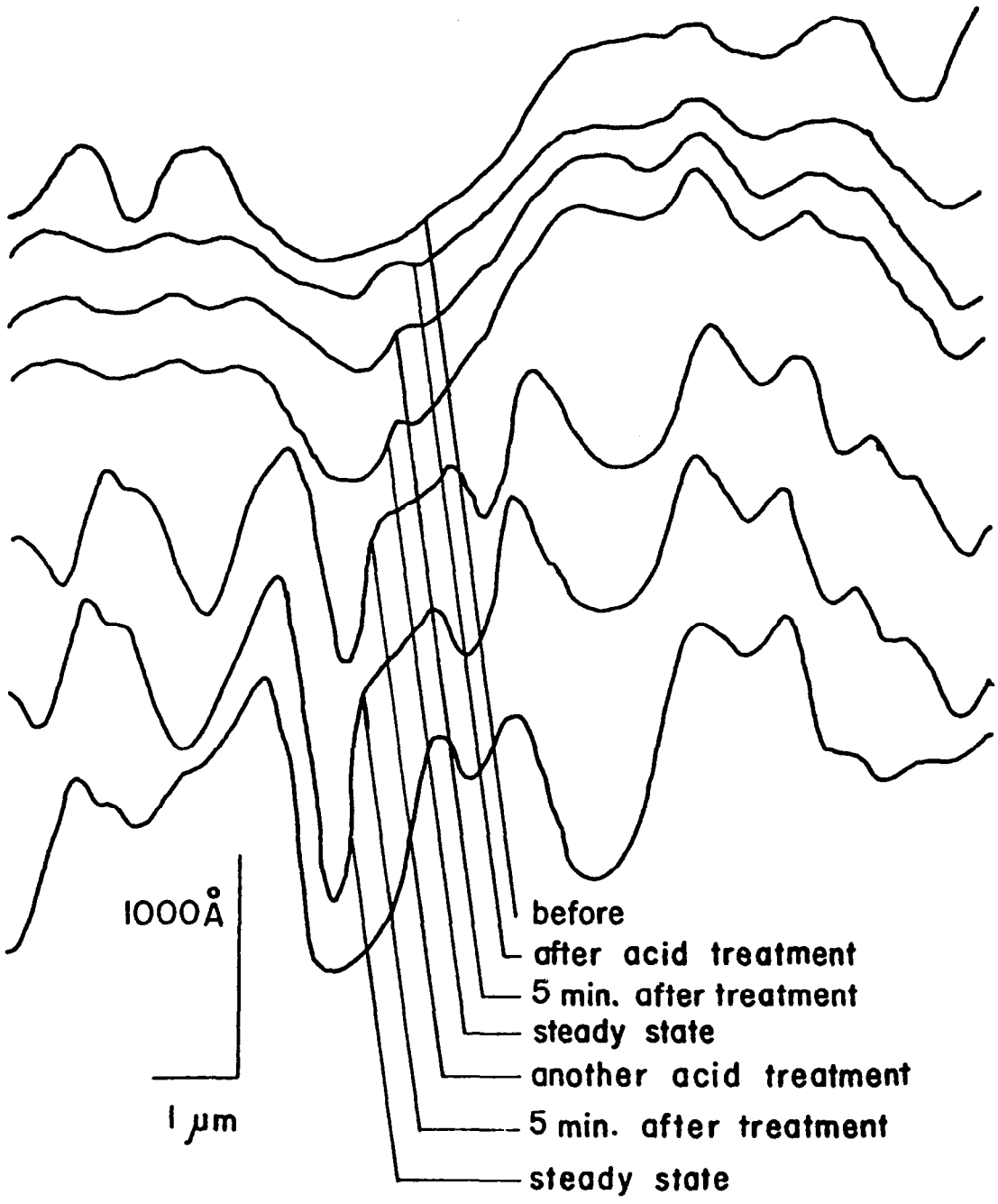

Figure 6.3 Series of Profiles of the Bearing Ball of Figure 6.2 Taken Outside of the Scuff Mark. Two successive probe treatments were given. (Profiles were set off to avoid overlap.)

6.1.3 Examinations of Ball Surfaces Run in Polyphenyl Ether Containing 1% of 1,1,2-Trichloroethane (TCE) with the P.L.I.M.

Figure 6.4 shows the profiles obtained with a bearing ball within and without the scuff mark, then the polyphenyl ether (5P4E) lubricant contained 1% of 1,1,2-trichloroethane (TCE). As can be seen, the differences of profile produced by the probe treatment were minimal in each case, although the changes within the track were a little bit more evident.

6.1.4 Examinations of Titanium-nitride-coated Bearing Ball Run in Polyphenyl Ether with or without 1,1,2-trichloroethane (TCE) with the P.L.I.M.

In this case, scuffing did not occur. The profiles outside the barely visible score mark did not change at all on probe treatment, but, with TCE and within the score, continuous changes occurred. It turned out to be impossible to get reproducible profiles under these conditions. For these reasons, we assumed that cracks in the coating has occurred. The following section shows a confirmation of this hypothesis by photographs taken under the scanning electron microscope.

6.1.5 Scanning Electron Photomicrographs of Wear Surfaces

Perhaps the most interesting of these photos is Figures 6.5 and 6.6 taken within and without the barely noticeable score mark of a TiN-coated ball. The light areas represent TiN coatings. The ladder-type structure within the score mark is very interesting and will be discussed later. The picture taken off the track shows the porosity of the TiN coating.

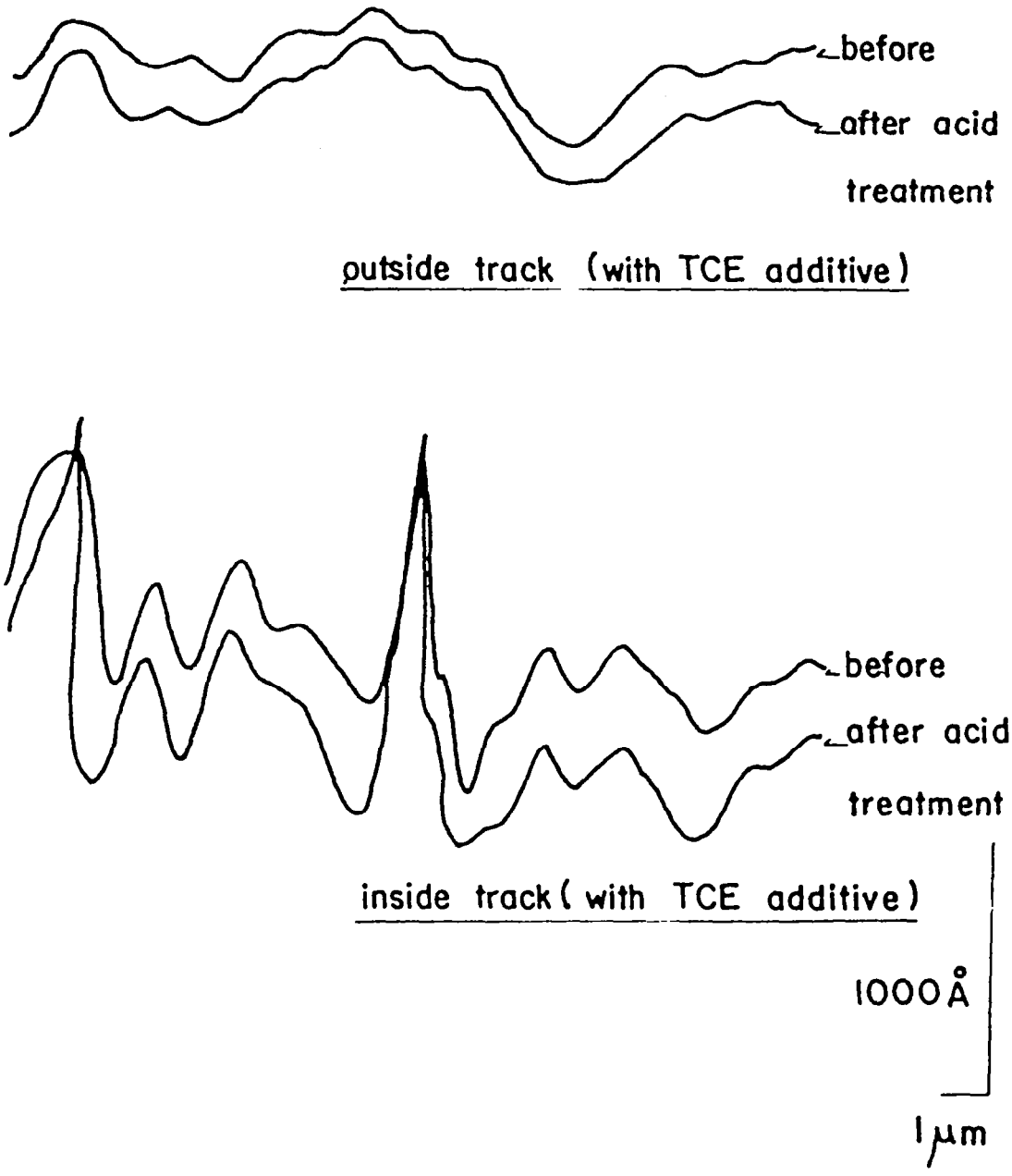

Figure 6.4 Surface Profiles of a Different Stainless Steel Bearing Ball Scuffed in Polyphenyl Ether Containing 1% of 1,1,2-trichloroethane. The top traces were taken outside the scuff mark, whereas the bottom traces were taken inside the scuff mark. (The traces recorded after the acid treatment were set off to avoid overlap.)

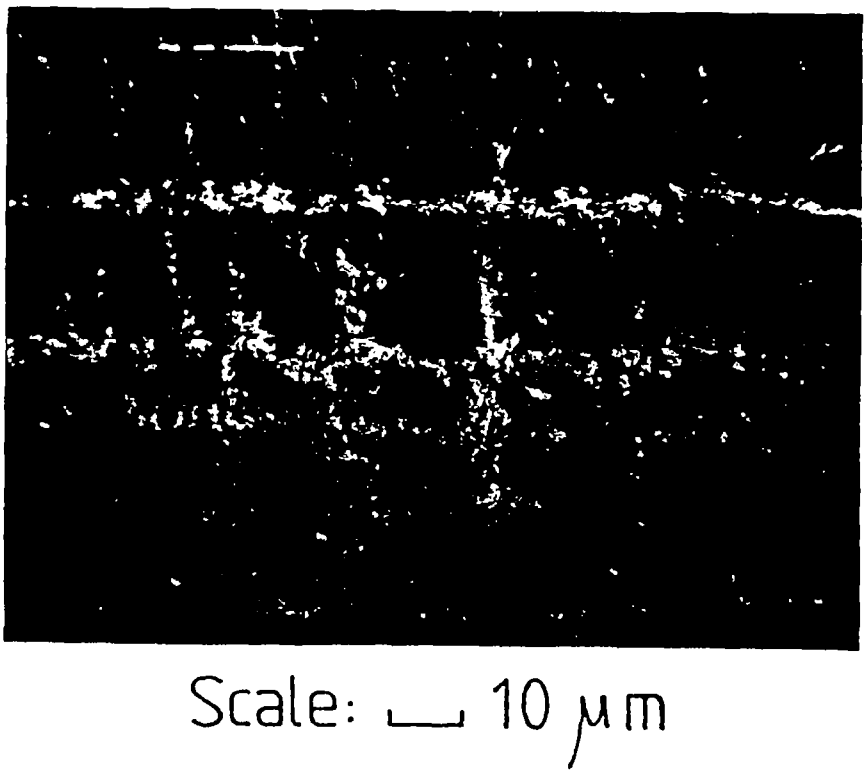

Figure 6.5 SEM of TiN-coated Ball Taken within the Score Mark, Note Ladder-like Porous Structure. The lubricant was polyphenylether (5P4E) with 1% of 1,1,2-trichloroethane.

Figure 6.6 SEM of TiN-coated Ball Taken Outside the Score Mark, Note Porous Structure. The lubricant was polyphenylether (5P4E) with 1% of 1,1,2-trichloroethane.

The electron photomicrographs of the bare ball after use with polyphenyl ether are also interesting. Without TCE, the wear track shows streaks and some of the characteristic scuff marks (Figure 6.7). When TCE was present, however, round specks occur with high concentration in the track of highest wear (Figure 6.8). Outside the wear track, these specks were essentially absent.

6.1.6 Profiles of Heated Plates Before and After Reaction with 0.04 M Alcohol Hydrochloric Acid

To answer the question whether the heating above a "total" temperature would change the reactivity, we applied the same alcoholic hydrochloric acid probe we used for the scuffed balls to heated steel specimens. The probe was, of course, applied at room temperature.

The test plates were prepared in the following manner. They were sandwiched in a holder between half-inch thick asbestos plates containing a three-quarter-inch diameter hole in the center. Two pieces of a material melting or changing color at known temperatures were clamped onto top side of the sample, allowing temperature monitoring during heating. The two temperature indicators were selected in such a way that the maximum heating temperature was bracketed between them; in other words, heating would be stopped when either of them melted or changed color.

Heating was accomplished rapidly (at 220 K/s) with the hot gases just above the tip of an acetylene flame directed at the lower side of the plates. At the same time and for a considerable time thereafter, nitrogen gas was blown over the top side of the plate to reduce or prevent oxidation (cooling rate: 100 K/s). Oxidation could never be

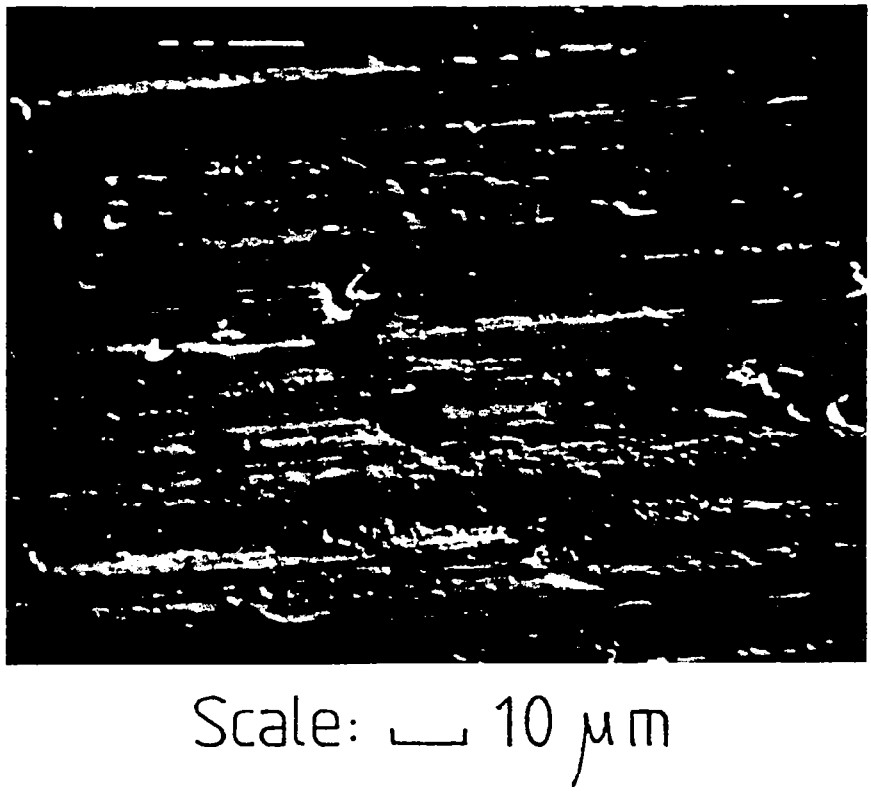

Figure 6.7 SEM of 440 C Steel Ball Run on Polyphenyl Ether to Scuffing. Note wear track with characteristic scuff marks.

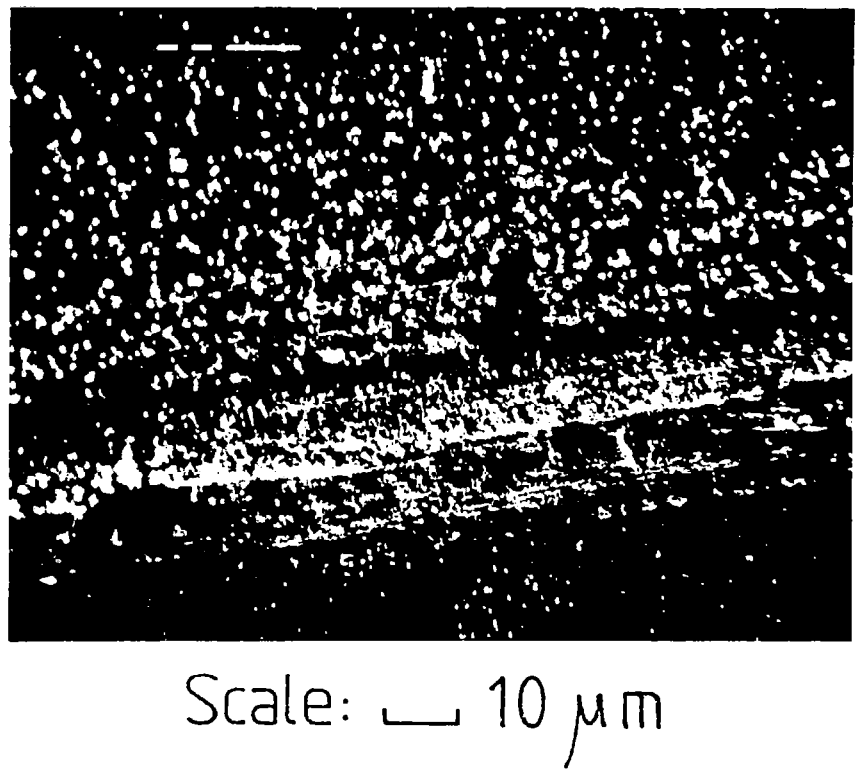

Figure 6.8 SEM of 440 C Steel Ball Run on Polyphenyl Ether Containing 1% of 1,1,2-trichloroethane. Note the round specks.

entirely prevented because vacuum was not used to remove adsorbed gas. On the other hand, one of the purposes of this work was the simulation of realistic field conditions, in which oxide films are never absent.

Figure 6.9 shows such profiles before and after treatment, when the plate was heated to 204°C and to 774°C. In the former case, the changes in contour were small; in the latter case, rather large.

The heating or "tempering" may have changed the microstructure of the steel and probably did so even though the metallurgically prescribed procedure was not followed.

Based on the changes in the contour for different samples heated to different temperature and then treated later with the acid probe, an Arrhenius-type plot of contour changes (the shaded areas of Figure 6.9, for example) against temperature was obtained. The discrepancies from an average straight line, considering the relative crudeness of the method, are not great (Figure 6.10).

6.2 Topographical Reaction Rate Versus Soaking or Operating Time with the P.L.I.M. Operating at More than One Wavelength

With the addition of an argon ion laser after the previous set of experiments, it is possible to use a number of wavelengths as surface probes. If the surface is metallic, such as gold or coated by a transparent oxide, such as aluminum oxide (Figure 6.11), the profiles are the same for different wavelengths. However, with steels usually covered by a light-absorbing oxide coating the profiles appear to be different (Figure 6.12). Since the oxide layers are known to be extremely thin, the same metal surface is always the source of sample reflection. The

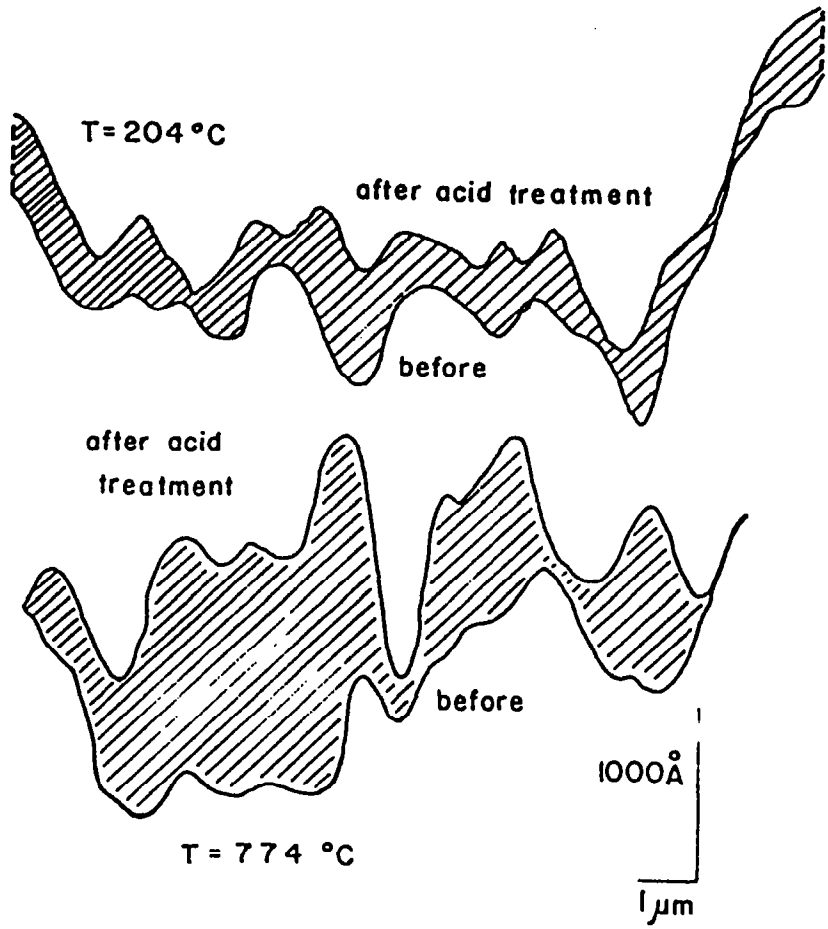

change in profile after acid treatment for heated specimen

Figure 6.9 Change of Surface Profile after Treatment with Alcoholic Hydrochloric Acid of a Stainless Steel Specimen Heated to (a) 204°C, and (b) 774°C

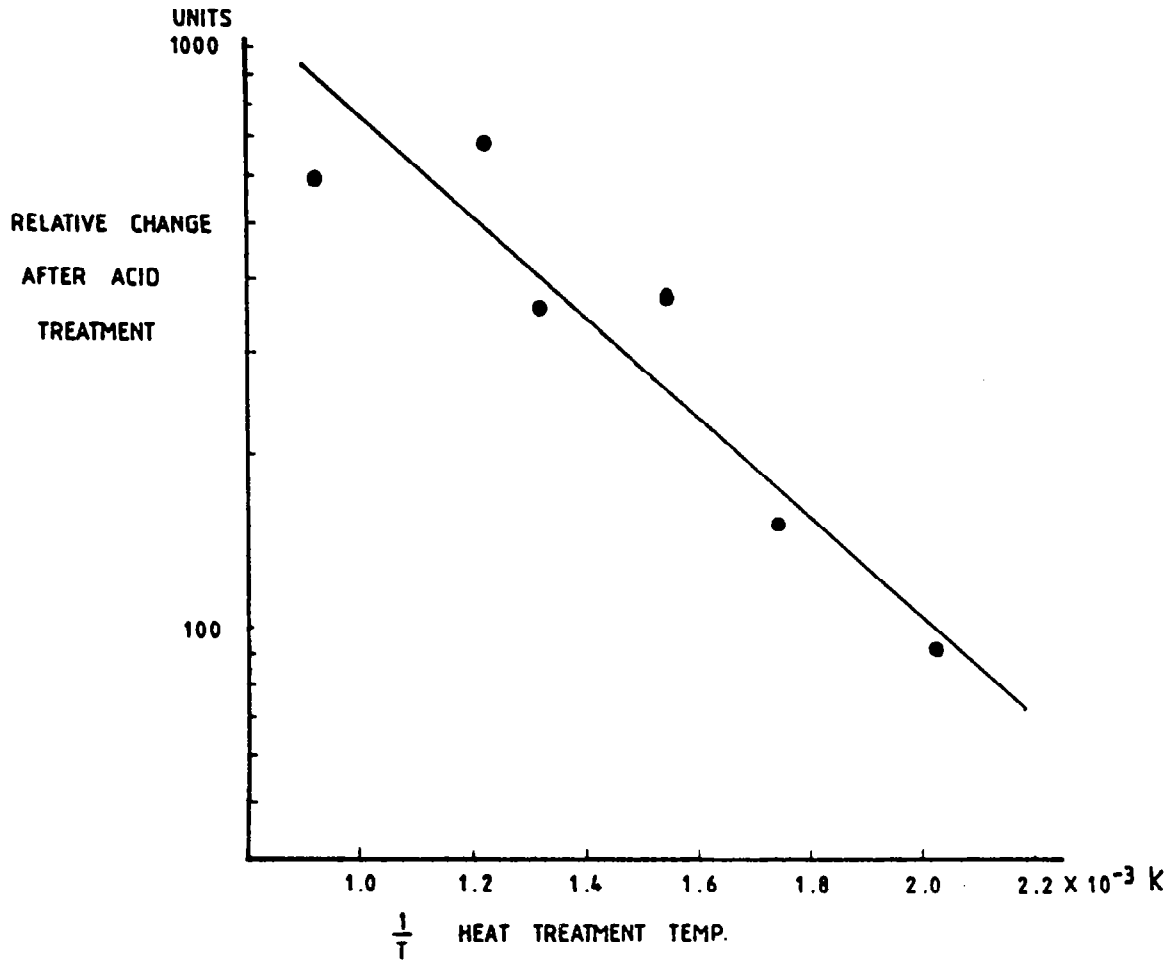

Figure 6.10 Arrhenius-type Plot of Surface Profile Change of Stainless Steel Specimens Heated to Different Temperatures. Relative surface change after acid treatment of S.S. (304) specimens heated to different temperatures.

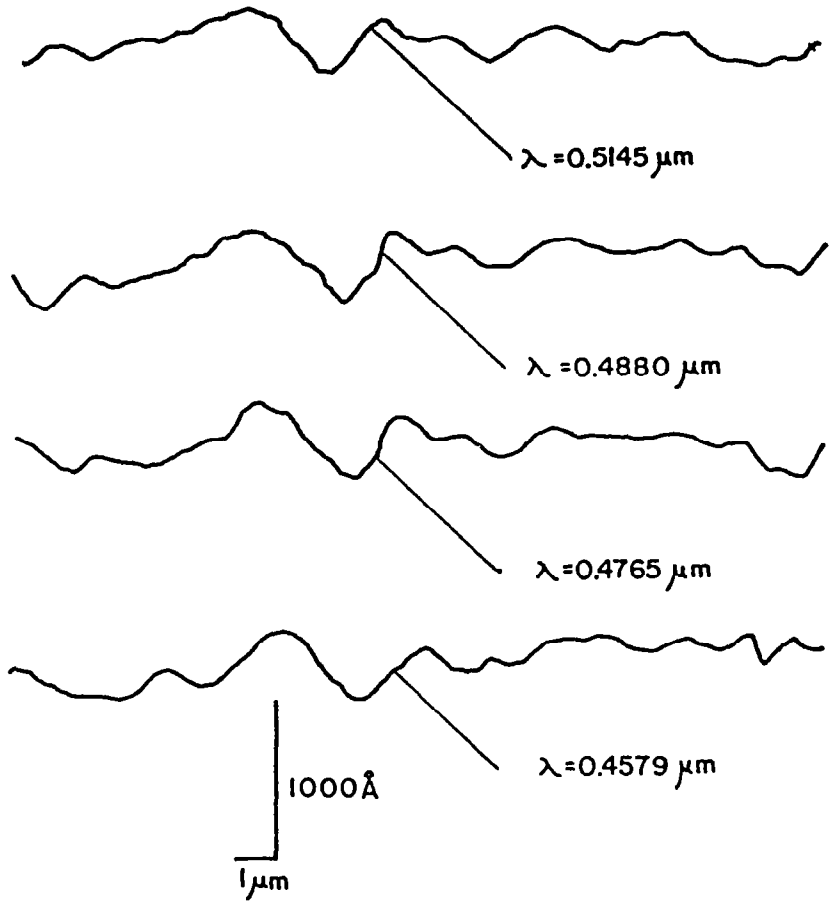

Figure 6.11 Optical Profiles of an Aluminum Plate Obtained with Different Wavelengths of an Argon Ion Laser

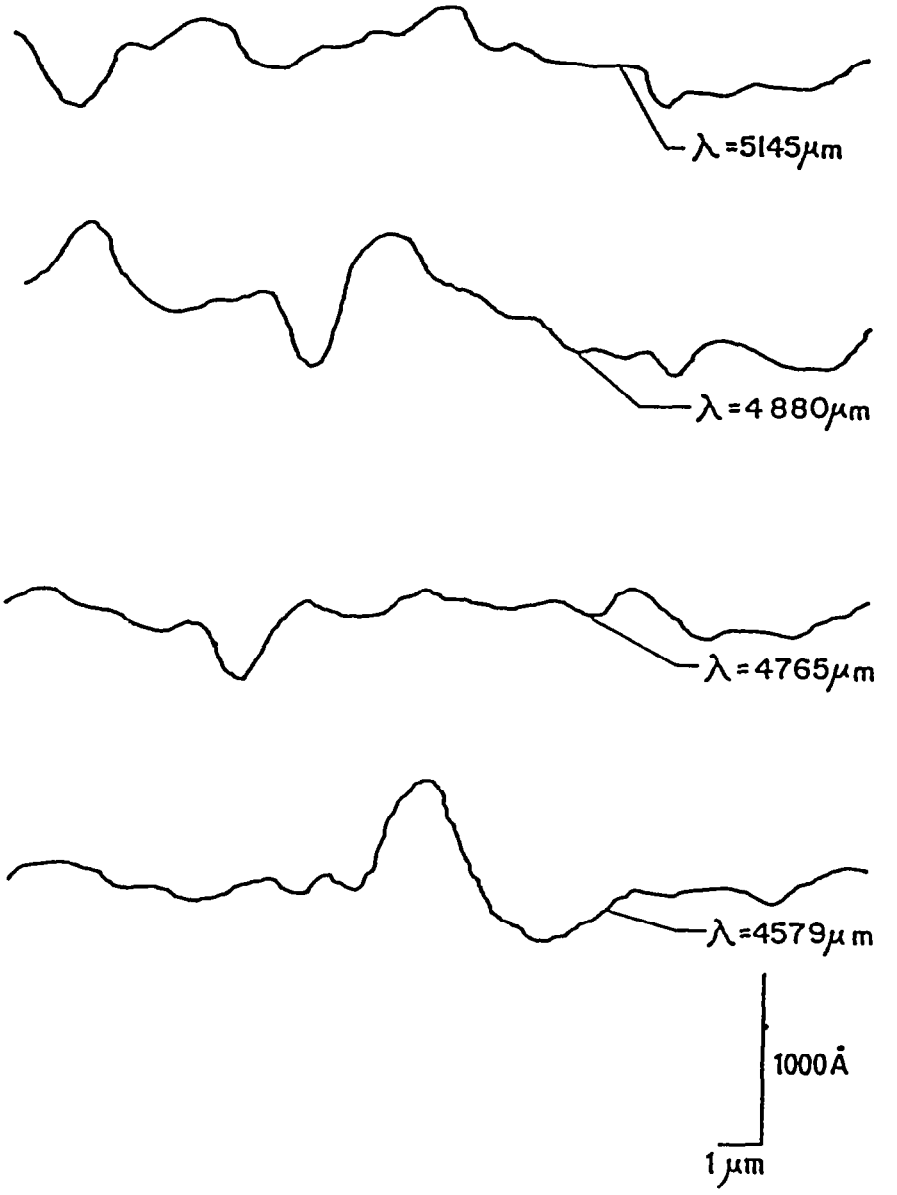

Figure 6.12 Optical Profiles of a Steel Plate Obtained with Different Wavelengths of an Argon Ion Laser

differences are therefore ascribed to phase changes on reflection, which are wavelength-dependent. When a wavelength is partially absorbed by the oxide (e.g., blue light by a red oxide), the phase change is dependent on the thickness of the oxide layer and significantly different from that produced by the pure metal. Therefore the "apparent depth profile" scanned by this wavelength which is not absorbed is different from that scanned by a wavelength. From this difference the thickness of the oxide layer can be calculated provided its optical parameters are known. In the following series of experiments, it is important to know that real profiles and apparent profiles are mixed. However, we are only measuring the relative changes. For this reason care must be taken not to imply that the observed profile changes are always true surface contour changes.

In the following experiments, two wavelengths, 5145 Å and 4880 Å were used to obtain the surface profiles as they were the more powerful lines from the laser. The reactivity data were obtained from the 4880 Å line.

6.2.1 Effect on Surface Profile of Surface Treatment with the Lubricant Trimethylolpropane Triheptanoate with and without Various Additives

The lubricant and its various additives are described in detail in Part 5. In this experiment a series of profiles were taken and the positions of the y-mirror were recorded. In other words, these profiles recorded were adjacent to each other. Then a drop of lubricant of interest was placed on the surface. After five minutes the surface was washed off with alcohol thoroughly. Another set of profiles similar to the original set were taken. Obviously, we cannot position

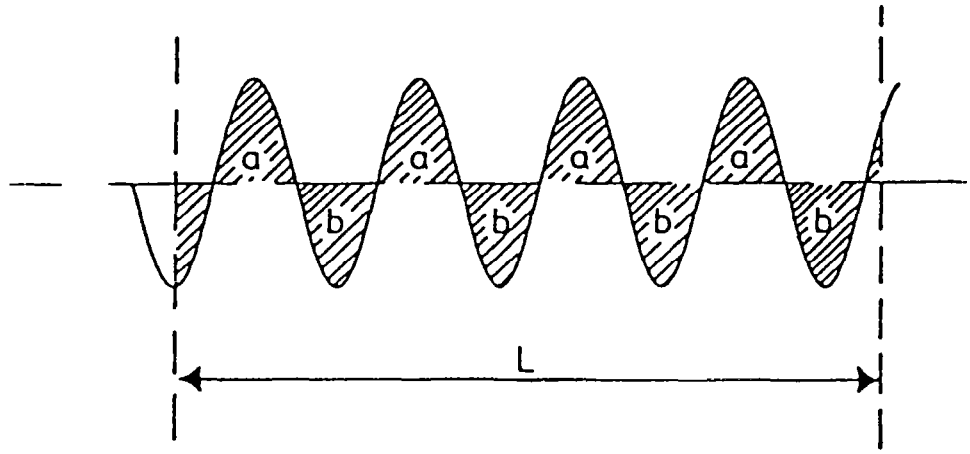

Figure 6.13 Definition of Centerline Average. Centerline positioned so that Σ (areas a) = Σ (areas b). The arithmetical mean deviation (formerly CLA) is defined by

$$\frac{\Sigma \text{ (areas a)} + \Sigma \text{ (areas b)}}{L \times \text{vertical magnification}}$$

the mirror to the exact position as before since there may be surface reaction which results in phase change. Finally, the acid treatment using the 0.011 M alcohol hydrochloric acid was applied and profiles were taken afterwards.

In order to evaluate the effect of these lubricants on the surface profile in general, a statistical measure was imposed. The area of a profile, as defined by the centerline average (Figure 6.13) was measured by a compensating polar planimeter. When an operator guides the planimeter through the perimeter of the shaded area in a clockwise direction, the shaded area can easily be measured.

Since the new bearing surface will always have different centerline average value as the statistical sample is not large enough, the CLA was normalized to zero for all cases. The effects of the different lubricant and acid treatment thereafter are summarized in Figure 6.14 with a histogram-type of presentation.

It can be seen that the different additives in the oil have different effects on the surface. For the base oil and the base oil with the BTZ and PANA additive, we can see that the surfaces in effect have been smoothened whereas the base oil with DODPA and TCP as well as the fully formulated oil G-MIL-99 actually roughen the surface. However, the effect of the oil to the surface is not as drastic as the roughening of the surface after the acid treatment. In all six cases, the surfaces were roughened as a result of the acid treatment. It appears that the acid treatment has a more drastic effect on the samples that have been treated by base oil with BTZ, DODPA and TCP. However, the fully formulated oil, which consists of all of the four additives, does not have

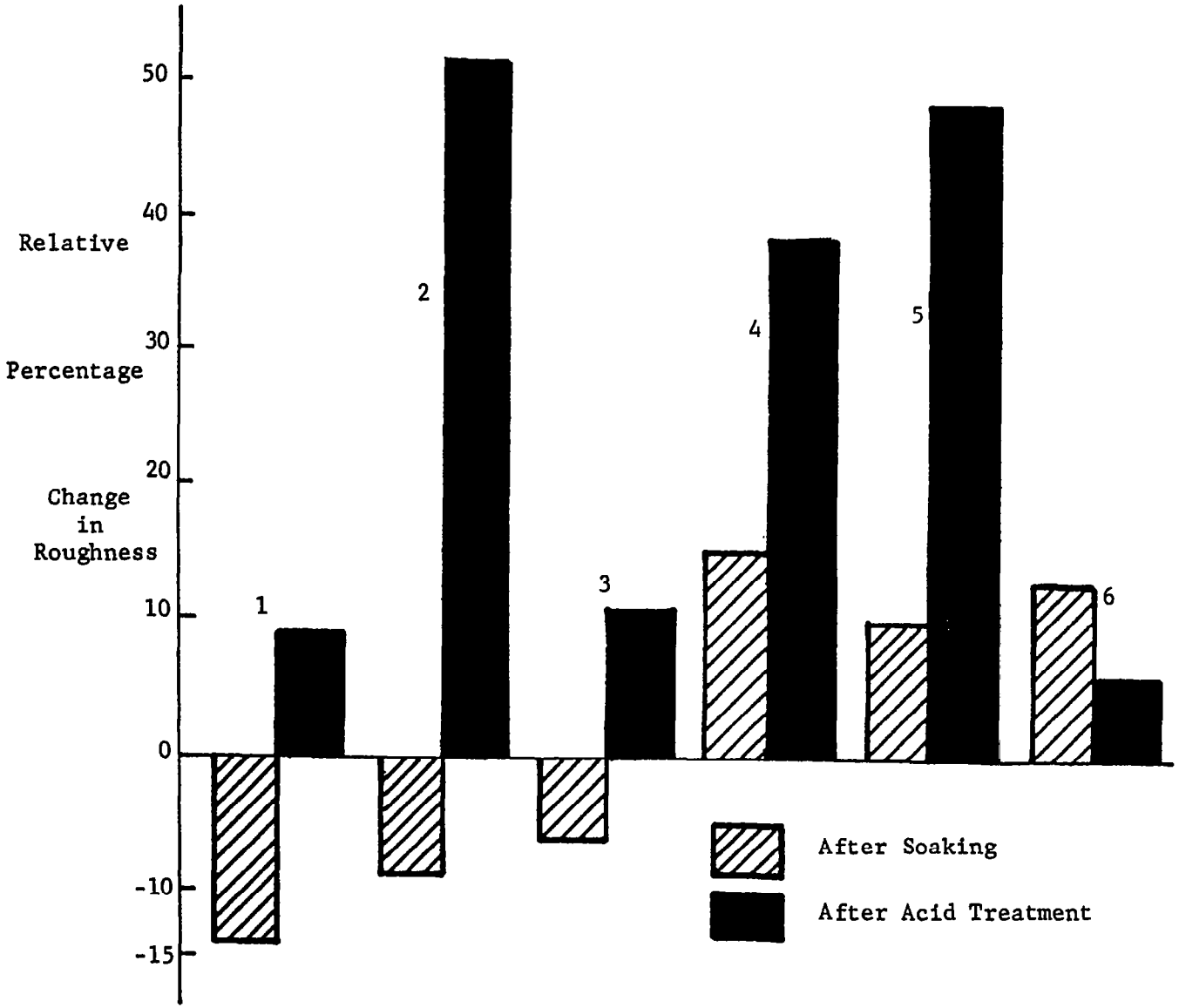

Figure 6.14 Relative Surface Roughness Change After Five-Minute Soaking and then Acid Treatment. (1 - Base oil; 2 - BTZ; 3 - PANA; 4 - DODPA; 5 - TCP; 6 - G-MIL-99. The original roughness is used as reference.)

much of an effect on the sample. Instead, the sample was actually smoothened relative to the soaking after the acid treatment.

6.2.2 Effect on Surface Profile of Surface Treatment with the Lubricant Containing 4.5% of Tricresyl Phosphate

As the additive tricresyl phosphate has received a great deal of attention, further investigation was done on this additive. Figure 6.15 shows the profile of the original M-50 plate surface as it was obtained with two different argon ion laser wavelengths. The surface was very smooth but the profiles show some differences with wavelength, which we attribute to patches of an oxide layer, for our experiments were carried out in the ambient atmosphere. For this reason the surfaces were very likely covered by adsorbed oxygen as well. The presence of adsorbed oxygen on M-50 steel in air was also inferred by Faut and Wheeler [30] from their experiments on the friction of TCP.

After contacting the same surface under the microscope with the TCP-containing lubricant for five minutes (Figure 6.16) at the same two wavelengths, there is little change in this particular surface profile. At the 4880 Å wavelength, the profile seemed to have smoothened. This is performed in an identical manner as the previous experiment. The profiles were obtained on dry surfaces - after exposure to lubricant the surface was rinsed with much alcohol and allowed to dry.

Another sample was soaked in TCP-containing lubricant for four days at ambient temperature before the profiles in Figure 6.17 were obtained using the 4880 Å wavelength. The profiles seem to be quite smooth in this case. A drop of 0.01 M hydrochloric acid in alcohol was

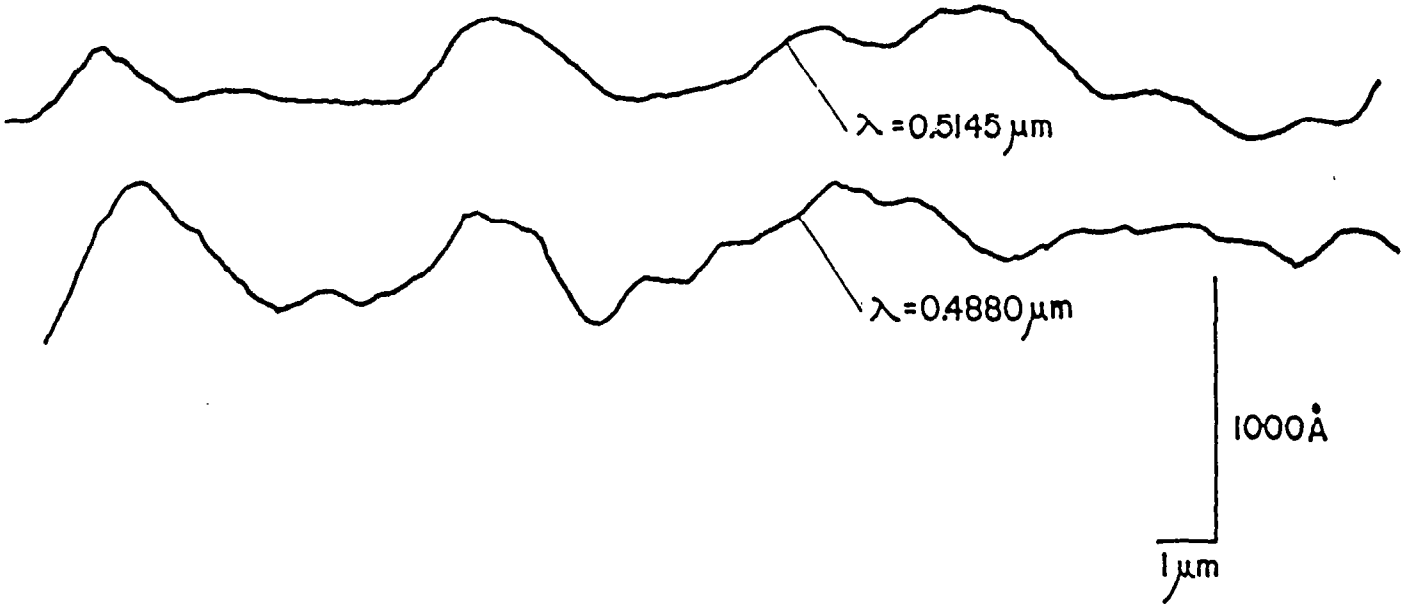

Figure 6.15 M-50 Plate Profile Before Tests. Profile difference with wavelengths are noted.

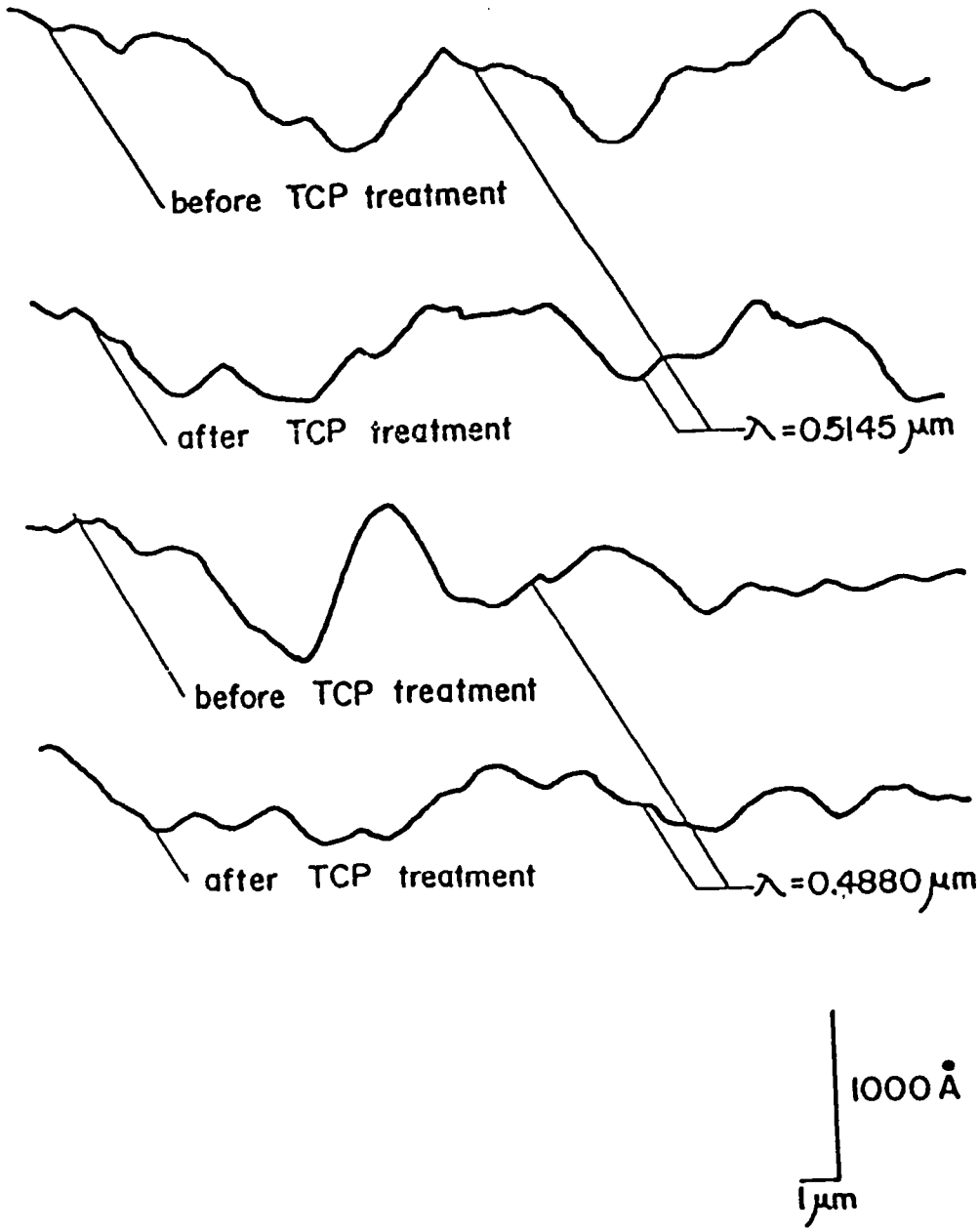

Figure 6.16 M-50 Plate Profile After Soaking for Five Minutes in Tricresyl Phosphate

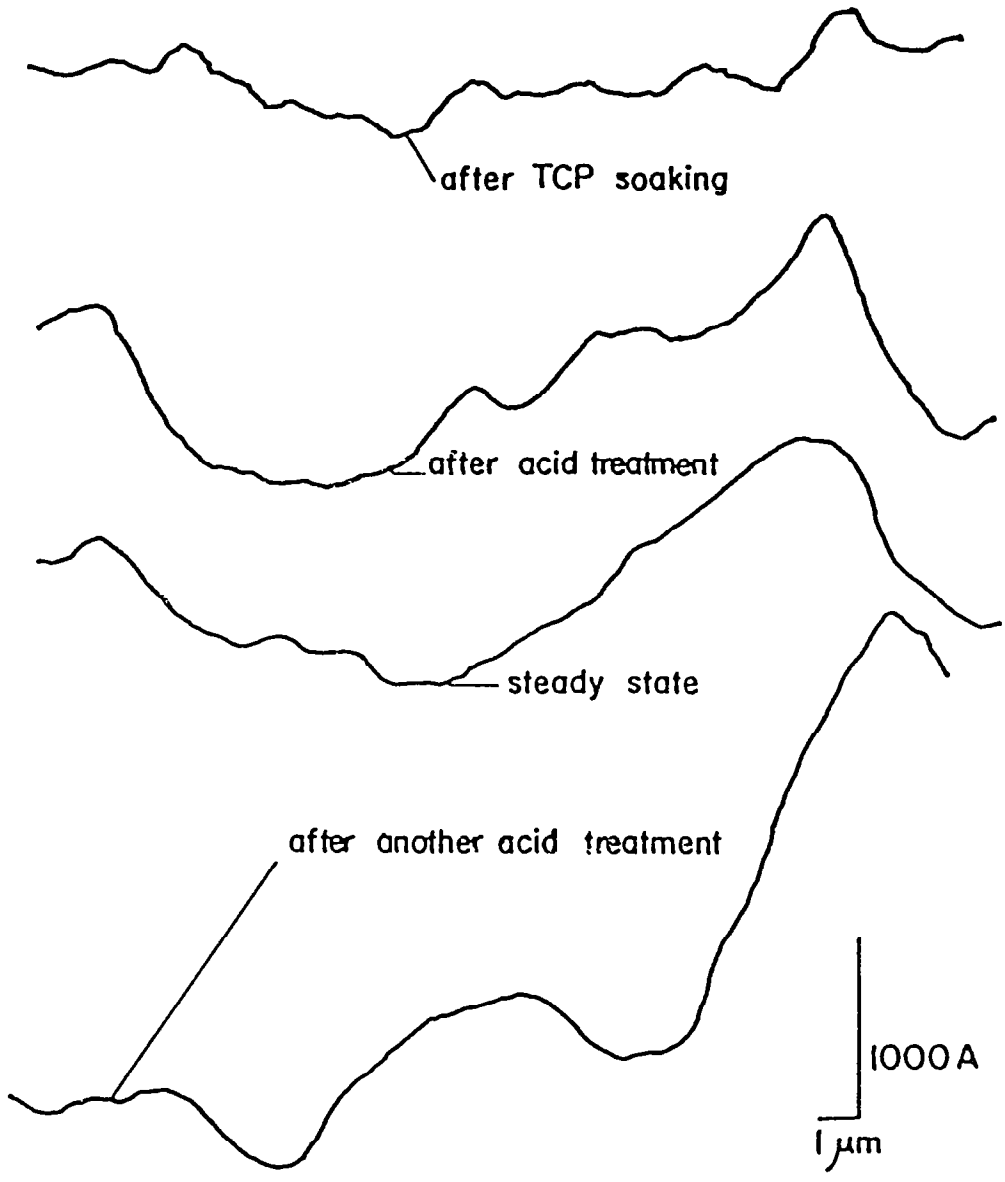

Figure 6.17 M-50 Plate Profile After Soaking for Four Days in Tricresyl Phosphate

applied for about ten seconds and then it was washed off. The small asperities were attacked and removed (base radii of 1 - 2 μm) but the larger ones were unaffected. The "steady state" situation was obtained after allowing the surface to rest for some time. It would appear that chemical reaction continued even after all the chloride was washed off. It could be more chloride formation, but it could also be oxidation subsequent to chloride formation. After another acid probe treatment one of the original small peaks had become a valley. However, the large features of the profiles remained.

To compare the TCP treated surfaces with untreated surfaces, the series of profiles of Figure 6.18 were obtained. Clearly, the changes after acid treatment are very small and even the acid of ten times the original strength did not change the profile very much. On careful examination of these profiles a certain long range periodicity of asperities is noticeable. The corresponding "wavelength" could correspond to an average grain size (Figure 5.1a,b). Interestingly enough therefore, the TCP-treated steel surface was much more reactive toward our probe (certainly for small asperities) than the untreated steel surface.

6.2.3 Reactivity of M-50 Surfaces as a Function of Running Time Toward Scuffing

The ball/plate bearing or sliding contact as described in the apparatus section was used to prepare samples. A bearing ball speed of 220 rpm or 0.22 m/s in linear speed was used throughout the experiment. A two-pound load was applied to the cantilever beam and it is equivalent to an average Hertzian pressure of 20 Kbar at the contact (Hertzian radius ~ 75 μm).

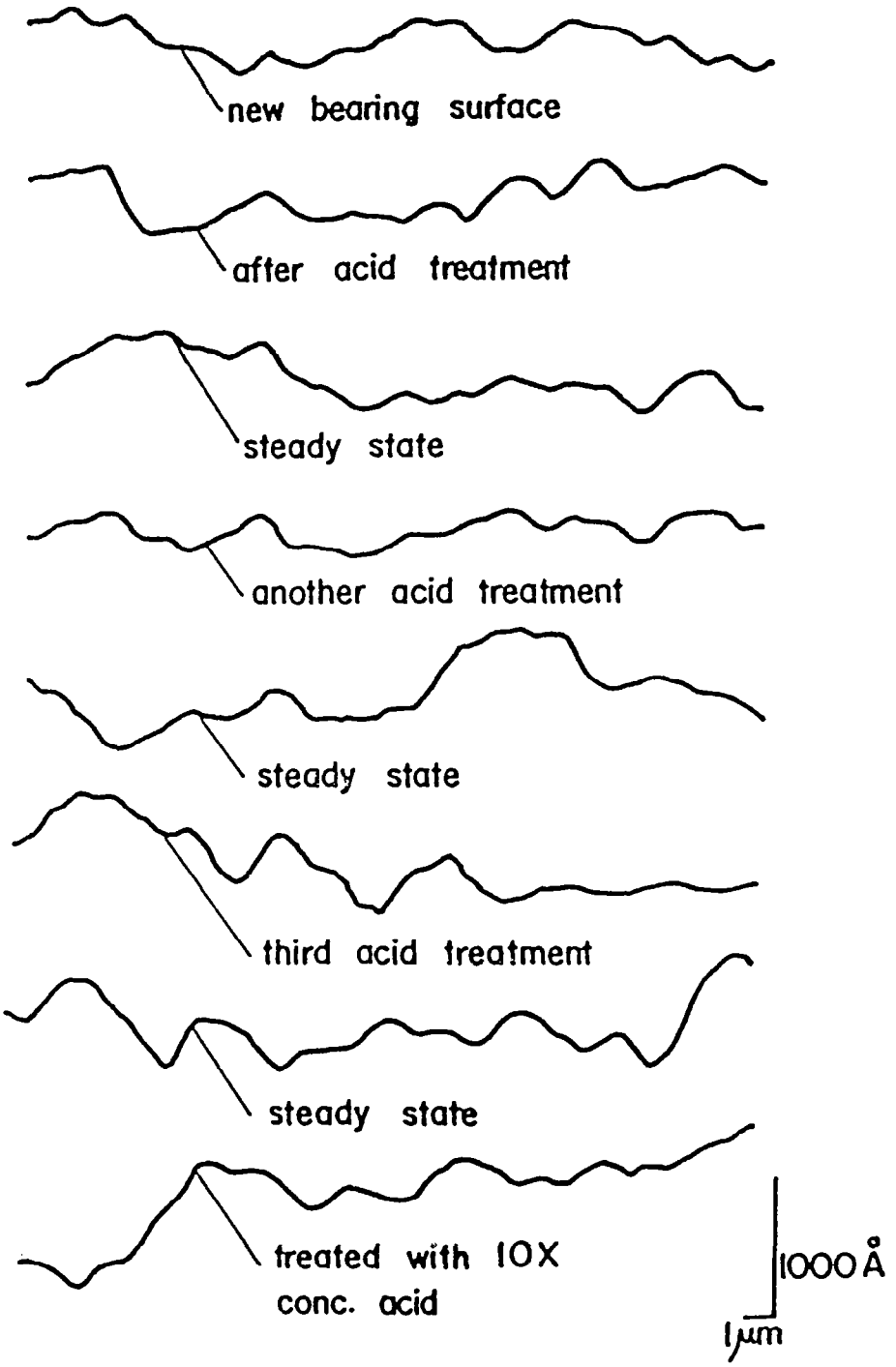

Figure 6.18 Series of Reactivity Test Profiles at 5145 Å of the Untreated M-50 Plate

Figures 6.19, 6.20 and 6.21 show plots of traction versus operating time under these conditions. The top two curves in Figure 6.19 correspond to the base oil containing the TCP and the bottom to the base oil alone. Both sets of plots also compare the effect of soaking the M-50 surface for three hours in the lubricant at ambient temperature. In the case of the base oil prior soaking merely extended the time to scuff from 120 sec to 400 sec, if scuffing is identified by the first steep rise of traction (subsequent examination of the wear track was consistent with this identification). The traction was somewhat reduced by the prior soaking, but not very much. In the case of the TCP-containing oil, prior soaking brought the traction to about the maximum value of the base oil; however, the traction was almost halved when soaking was eliminated. On the other hand, without soaking the traction was very erratic over the course of the experiment, exhibiting steep rises as well as drops. It was difficult to obtain reproducible running times toward scuffing in that case.

Comparison of the traction curves of Figure 6.19 shows a sharp increase near 400 sec for all cases except the base oil without soaking. As this increase apparently corresponds to scuffing, it would seem that TCP, in general, does not delay scuffing.

Other additive-containing base oils and the fully formulated oil were used subsequently in the reactivity study. The traction curves for dioctyldiphenylamine (DODPA), benzotriazole (BTZ), phenyl-alpha-naphthylamine (PANA) and the fully formulated oil (G-MIL-99) are shown in Figures 6.20 and 6.21. The samples in the following experiments were all soaked in their respective oil for three hours in ambient temperature

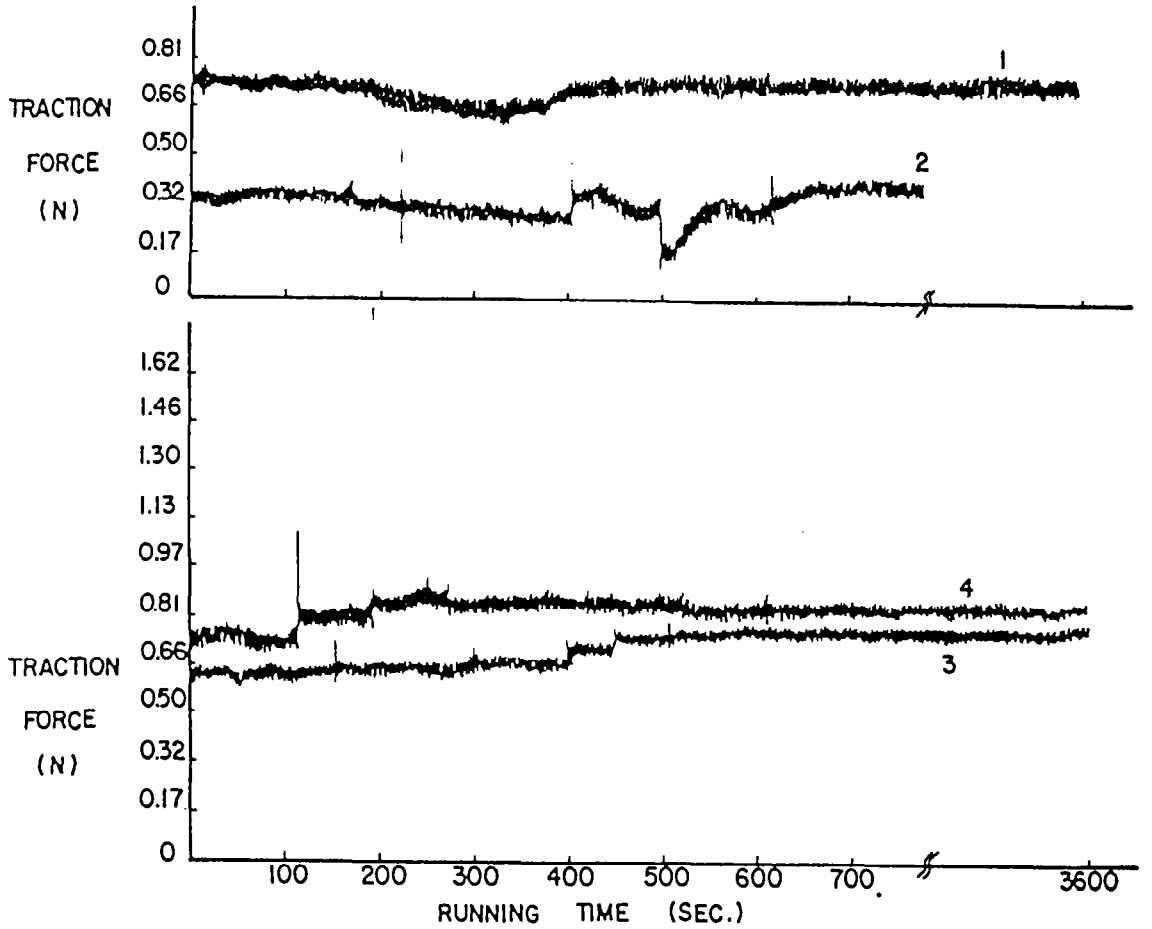

Figure 6.19 Traction Versus Time of Ball/Plate Contact Operation. These are recorder traces of independent experiments. Traces 1 and 2 refer to base oil with tricresylphosphate (TCP) additive, the former with three hours of prior soaking at ambient temperature, the latter without soaking. Traces 3 and 4 are the corresponding traces for the base oil without TCP. The inversion of the numbers of the two pairs and the upward step at 400 sec of all traces but 4 should be noted.

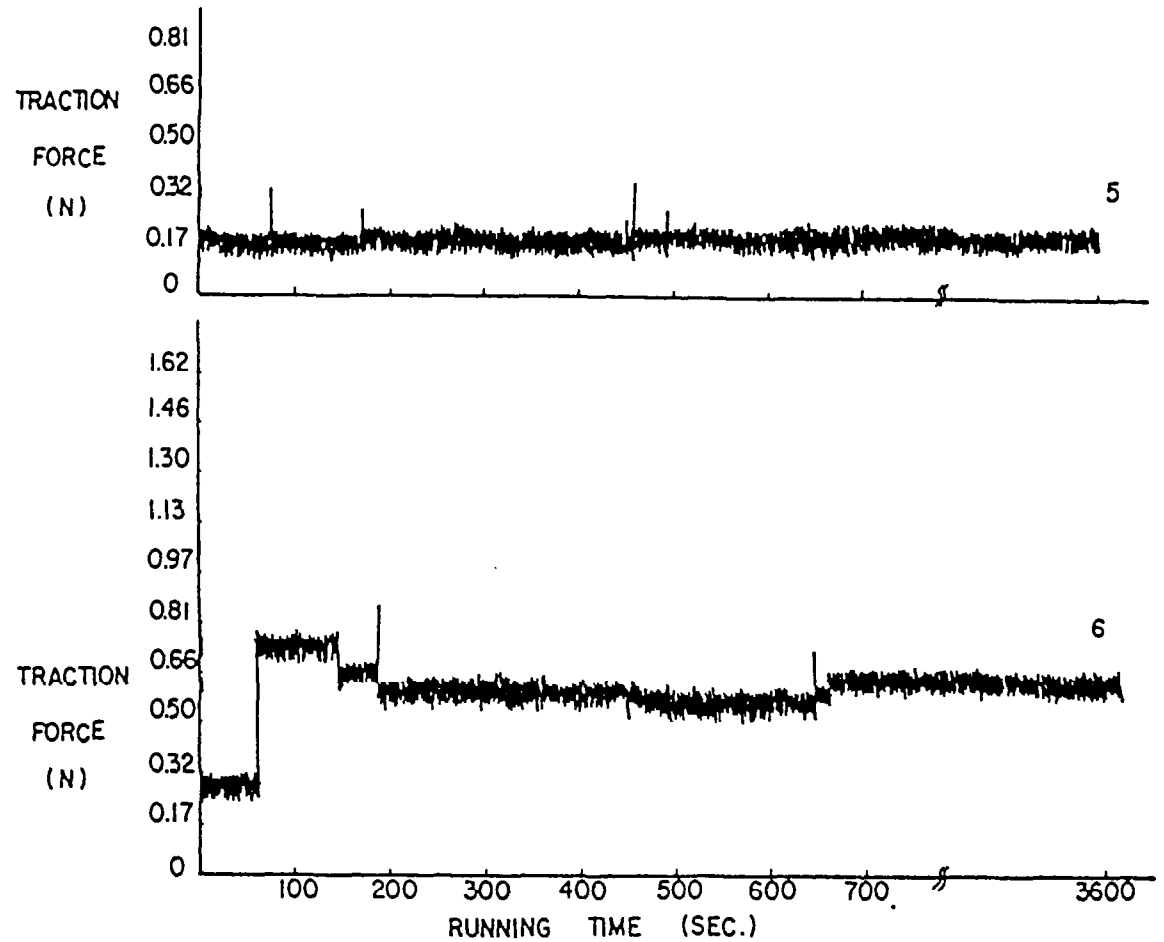

Figure 6.20 Traction Versus Time of Ball/Plate Contact Operations with Base Oil Containing (5) DODPA and (6) BTZ

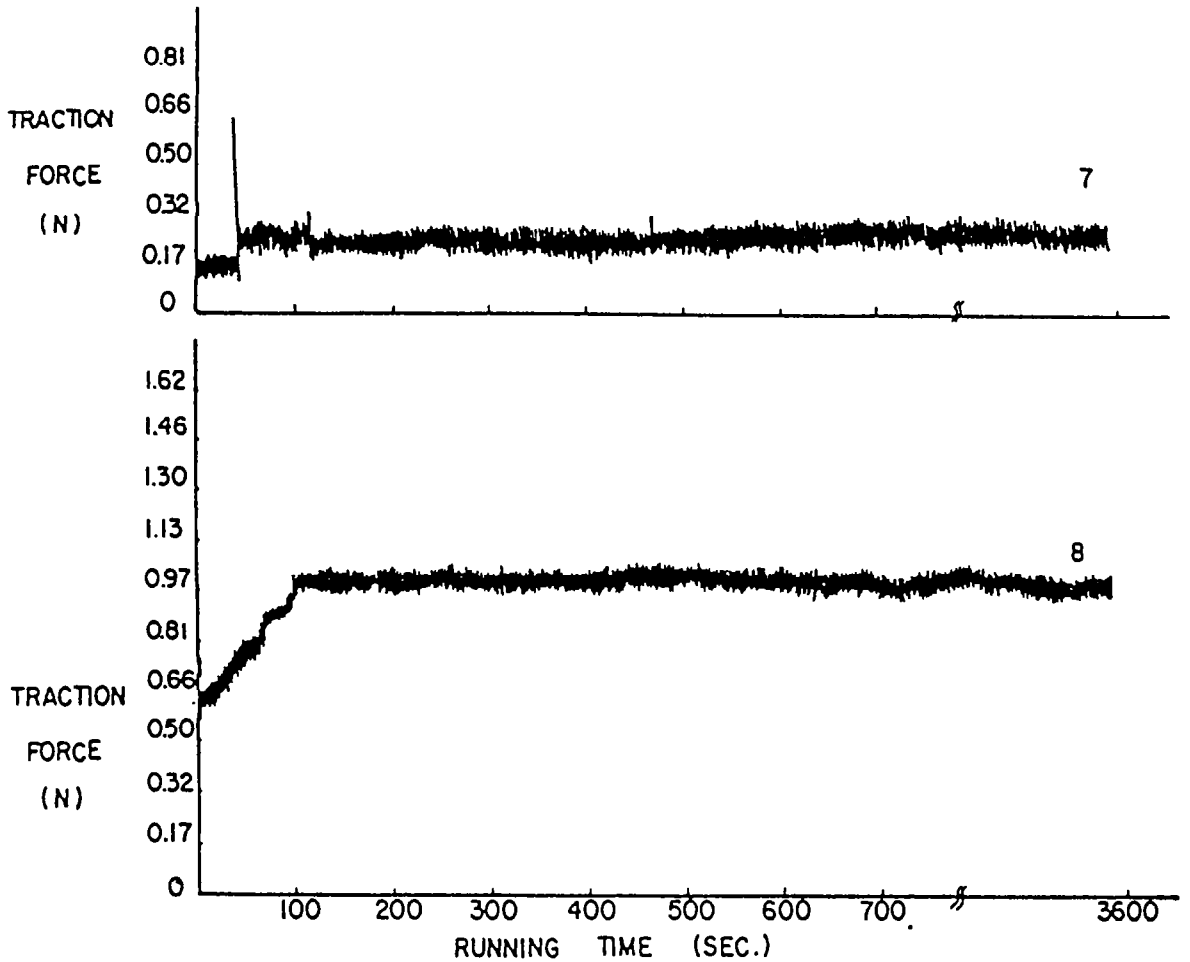

Figure 6.21 Traction Versus Time of Ball/Plate Contact Operation with Base Oil Containing (7) PANA and Fully Formulated Oil G-MIL-99

prior to running. As in the figures, curves No.5 and 7, which correspond to the two antioxidant additives DODPA and PANA, show a decrease in traction compared to the base oil or the base oil with TCP. Scuffing also occurred quite early in the case of PANA. (The sudden jump is found in less than one minute.) Curve No.6 corresponds to the experiment run with the base oil containing the corrosion inhibitor BTZ. A sudden increase in traction can be seen about one minute into the experiment, and is followed by a few steps exhibiting a decrease in traction force. Curve No.8 in Figure 6.21 is quite different in the sense that it shows a gradual increase in traction. Furthermore, it has the highest traction of all the runs. The gradual increase in traction may indicate that a running-in process is taking place.

Figure 6.22 shows a series of profiles within the wear track of the plate contact before and after acid treatment for zero, 20 sec, 40 sec, and 60 sec (after scuffing in this particular experiment). The time to scuffing did not always reproduce of running time. It is clear that the reactivity of the plate contact changed continuously with running time and became particularly large after scuffing. For example, the asperity of the next to the last profile (after scuffing) became a valley on acid treatment.

The profiles of Figure 6.22 were obtained with the base oil lubricant without soaking prior to running. When the profiles before acid treatment are examined as a function of running time, a slight increase of roughness can be seen up to the scuffing transition, which is accompanied by a large increase of roughness. The average roughness of the contact after different periods of operating time with various

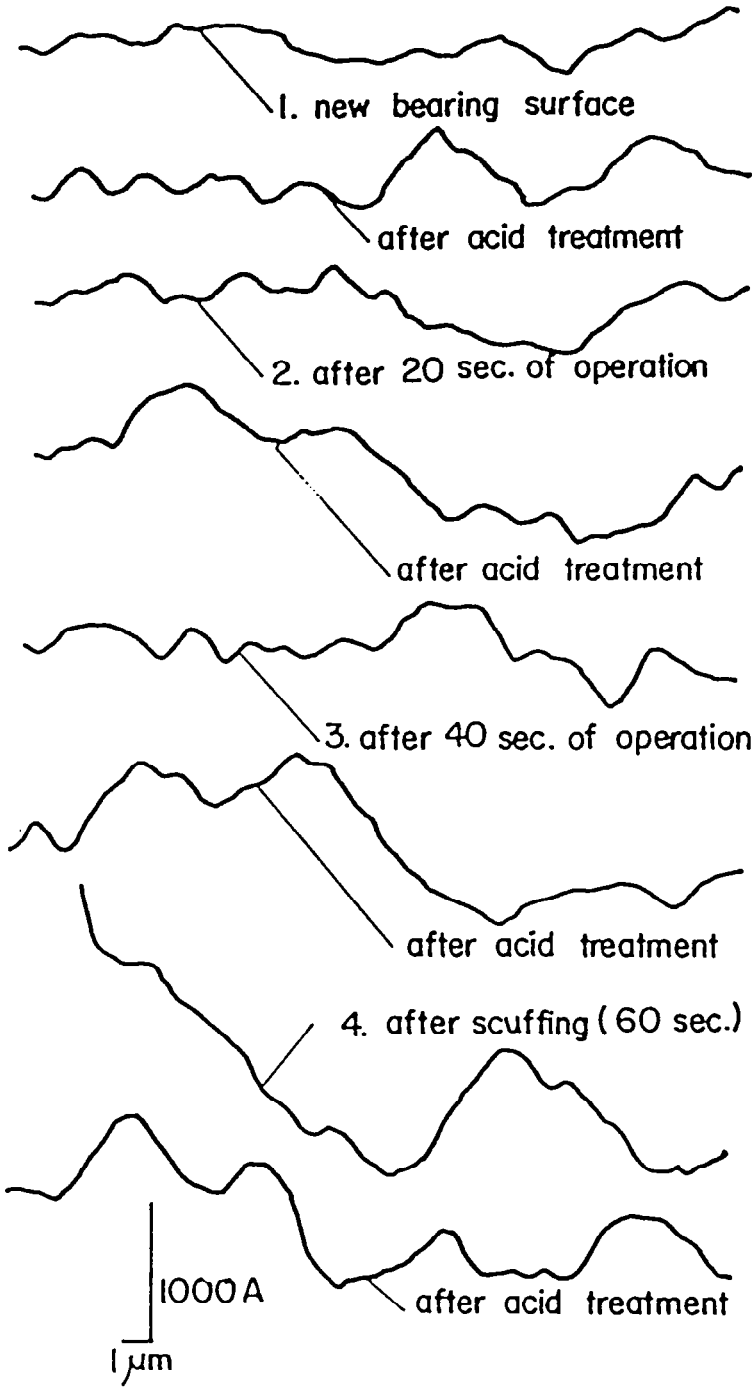

Figure 6.22 Surface Profiles within the Wear Track of M-50 Plate as Scuffing Conditions were Approached. The wavelength was 4880 Å and the temperature was ambient.

oils are shown in Table 6.1. Since a fairly small sample is obtained (usually five to six profiles with each profile being 20 μm long) for this purpose, one cannot interpret too much from these data. However, we can see that there is a trend of increasing roughness for the base oil case. With the TCP-containing oil experiment, the surface roughness increases gradually until it levels off at 40 sec with an average roughness of approximately 430. For the other cases, there is quite a fluctuation and we cannot extract any information from them other than that they were quite random.

In order to evaluate the profile changes produced by the acid probe reaction and thus get a measure of the surface reactivity toward alcoholic hydrochloric acid the centerline average method was again used. The method was explained in the previous section and the change of roughness so defined is a function of the action of the acid with respect to the surface. Figure 6.23 shows plots of these roughness changes produced by the acid probe as a function of operating time for three of the conditions of Figure 6.19. Without soaking and with only the base oil used, the reactivity is seen to increase very rapidly corresponding to the early scuffing noted in Figure 6.19. With soaking the reactivities prior to scuffing are greater when TCP is present, but the sharp increase of surface reactivity subsequent to scuffing occurs at nearly the same time for both the TCP-containing oil and the base oil after 2 min of operating time. The reactivity change for the contact after one hour is not a true representation of what actually happened for the following reason: the surface would become exceedingly rough as a result of scuffing (see Table 6.1) and any acid treatment would either make it rougher in around

TABLE 6.1*

AVERAGE ROUGHNESS OF M-50 BEARING SURFACE AFTER VARIOUS PERIOD OF OPERATING TIME WITH BASE OIL AND BASE OIL CONTAINING VARIOUS ADDITIVES (WITH SOAKING)

	0 sec	10 sec	20 sec	40 sec	1 min	2 min	1 hr
Base oil	245 ± 62	347 ± 72	420 ± 89	448 ± 69	687 ± 148	589 ± 90	645 ± 110
TCP	264 ± 72	246 ± 48	291 ± 88	482 ± 42	460 ± 83	432 ± 56	401 ± 130
DODPA	360 ± 80	306 ± 66	412 ± 52	314 ± 35	308 ± 49	283 ± 26	427 ± 76
PANA	443 ± 74	322 ± 86	459 ± 129	314 ± 45	281 ± 95	349 ± 49	403 ± 67
BTZ	406 ± 150	341 ± 55	271 ± 27	435 ± 62	513 ± 105	318 ± 40	519 ± 126
G-MIL-99	436 ± 35	419 ± 96	598 ± 130	355 ± 152	551 ± 125	296 ± 185	661 ± 227

* The average roughness was measured by the centerline average method and the profiles were obtained at 4880 Å wavelength.

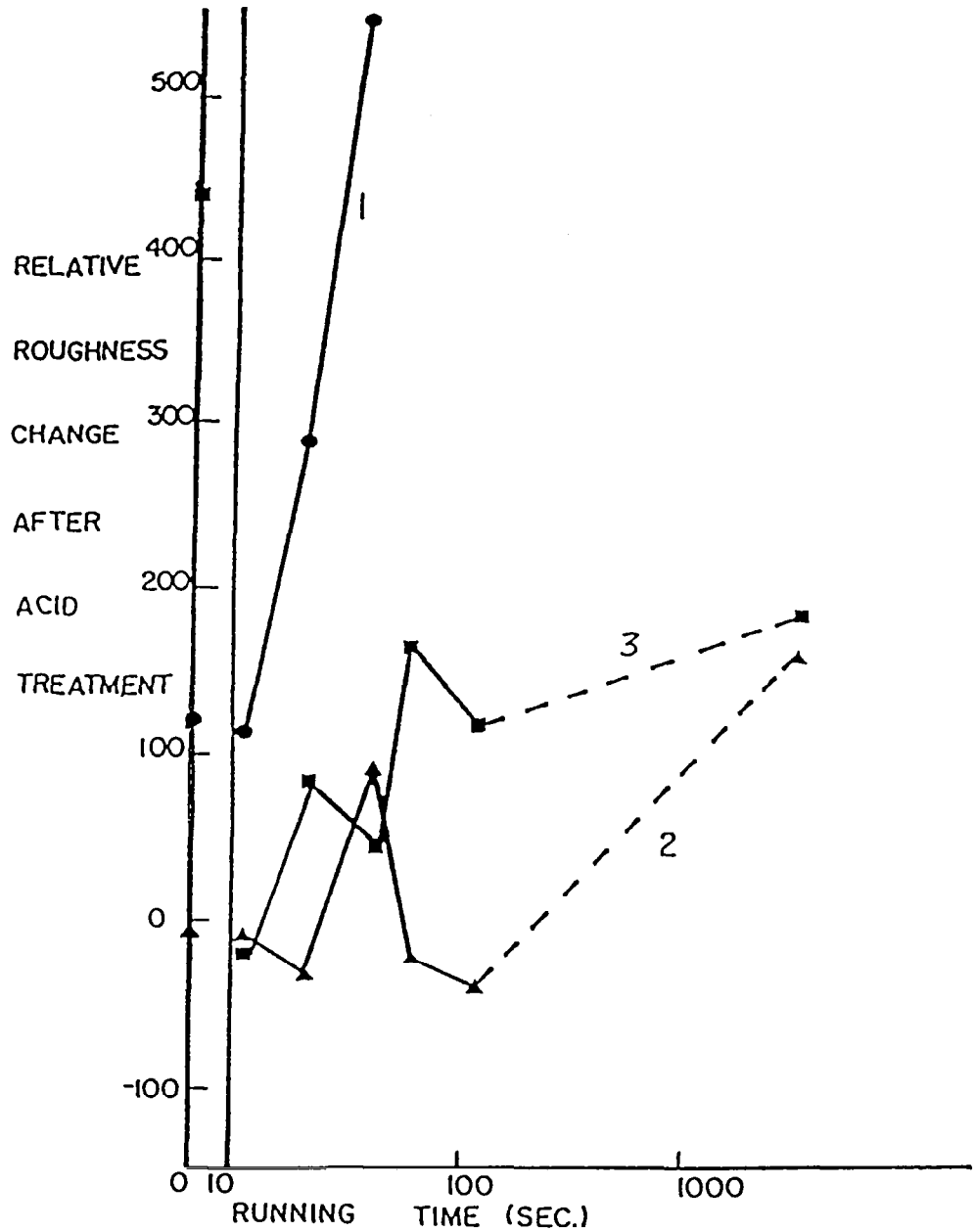

Figure 6.23 Effect of Acid Probe on Contact Region Roughness as Scuffing Conditions were Approached Using Base Oil with and without TCP. Curves 1, 2 and 3 represent base oil without TCP or prior soaking, base oil with TCP and prior soaking for three hours at ambient temperature, respectively.

the same order of magnitude or have rougher changes which is out of the range of what the instrument can measure - we will start to get phase jumps. Therefore the reactivity at that point is connected to the other points by way of a broken line.

Figure 6.23 also shows the very high reactivity toward the acid probe of the TCP-soaked surface before any running at all. It is higher than any reactivity noted after running.

A similar phenomenon can be found in Figure 6.24 where the situation is reversed. With the DODPA-containing oil, there is a high reactivity after 10 sec of running compared to no running at all. A slight dip follows before a gradual increase in reactivity. In the same figure the reactivity of the surface run with BTZ-containg oil is illustrated. During the first two minutes of operating, the reactivity of the surface is quite low compared to after an hour. Scuffing probably occurred after two minutes (see Figure 6.20) and it resulted in the high reactivity.

The reactivity for PANA-containing oil and the fully-formulated oil G-MIL-99 are illustrated in Figure 6.25. The PANA-containing oil, which is also in the same category as DODPA working as an antioxidant, shows the same kind of characteristics as DODPA. The reactivity increases with operating and it also decreases with extended period of operation. As mentioned earlier, the reactivity of the one hour point is somewhat questionable; therefore the two curves, DODPA and PANA both being anti-oxidant, may actually have the same shape of curve. On the other hand, the reactivity of the fully-formulated oil fluctuates near the zero line throughout the entire operating period. Apparently, the different

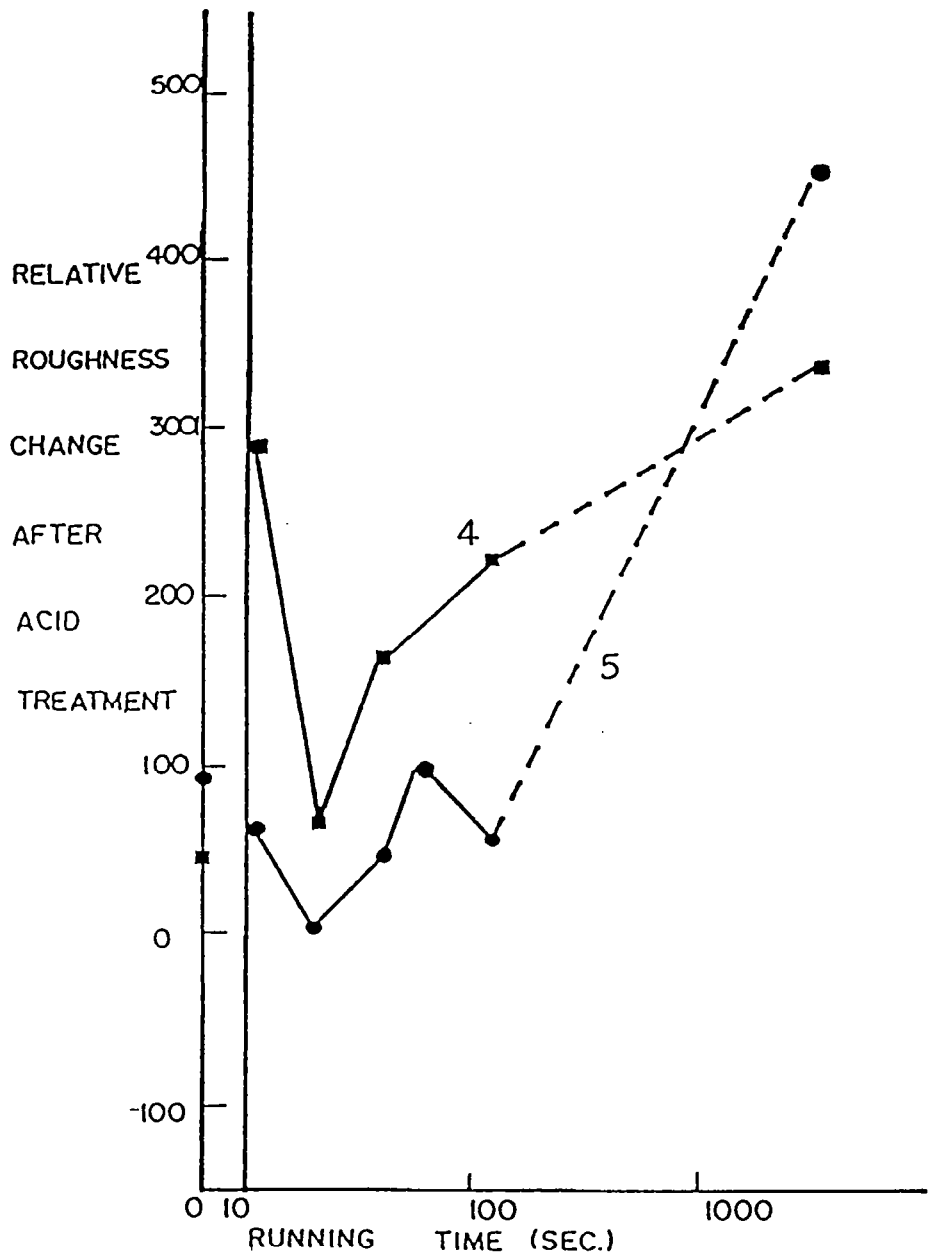

Figure 6.24 Effect of Acid Probe on Contact Region Roughness as a Function of Operating Time Using Base Oil with (4) DODPA and (5) BTZ

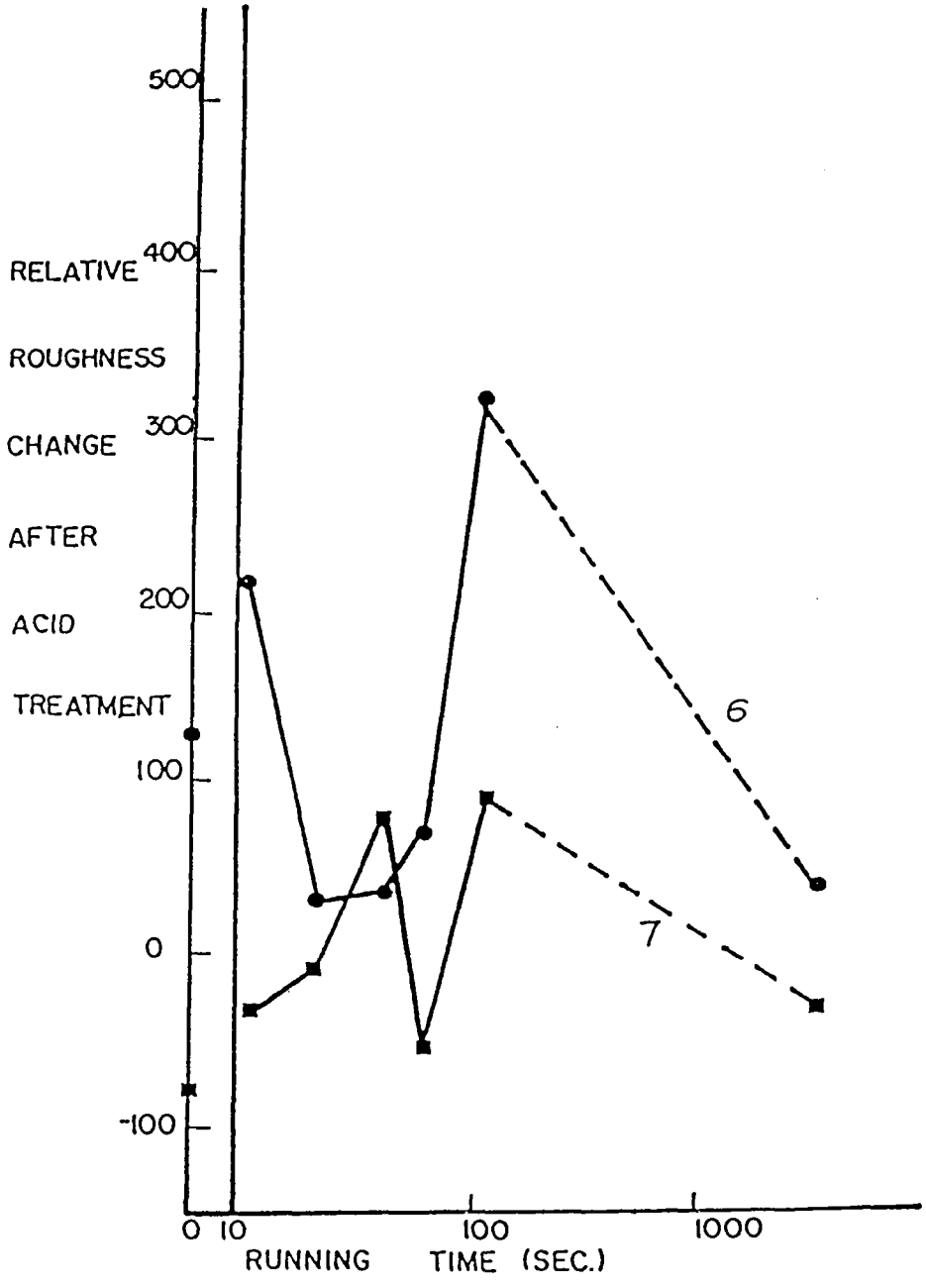

Figure 6.25 Effect of Acid Probe on Contact Region Roughness as a Function of Operating Time Using Base Oil with (6) PANA and the Fully-Formulated Oil (7)

additives, when combined, work together quite well and produce a lubricant which gives a low reactivity surface.

6.3 Metallurgical Study of Scuff Mark

In order to investigate the nature of the material in the scuff mark further, a plate was barely polished and etched with nital. Figure 6.26 shows that the material within the mark did not etch. The half-circular appearance of the mark would seem to indicate that the normal to the plate made a slight angle with the direction of the load. The rhombic shaped mark was caused by microhardness testing. The hardness inside and outside the mark were found to be the same, although the non-etching phase may be so thin that the hardness test was unable to pick up any differences. When the plate was polished a little bit more, the unetched material disappeared, even though some of the grooves still remained.

6.4 Other Instruments Utilized to Investigate the Scuff Mark

Other instruments, including the X-ray energy spectrometer, and the Auger spectrometer were used to study the scuff mark. Using the X-ray energy spectrometer did not yield any useful information. Investigations using the scanning Auger spectrometer are underway. However, it is quite a slow process because it involves the cutting of the sample into the proper size by using electrical discharge machining, and the low contrast of the scanning Auger viewing system makes it difficult to identify the scuff mark in the vacuum chamber.

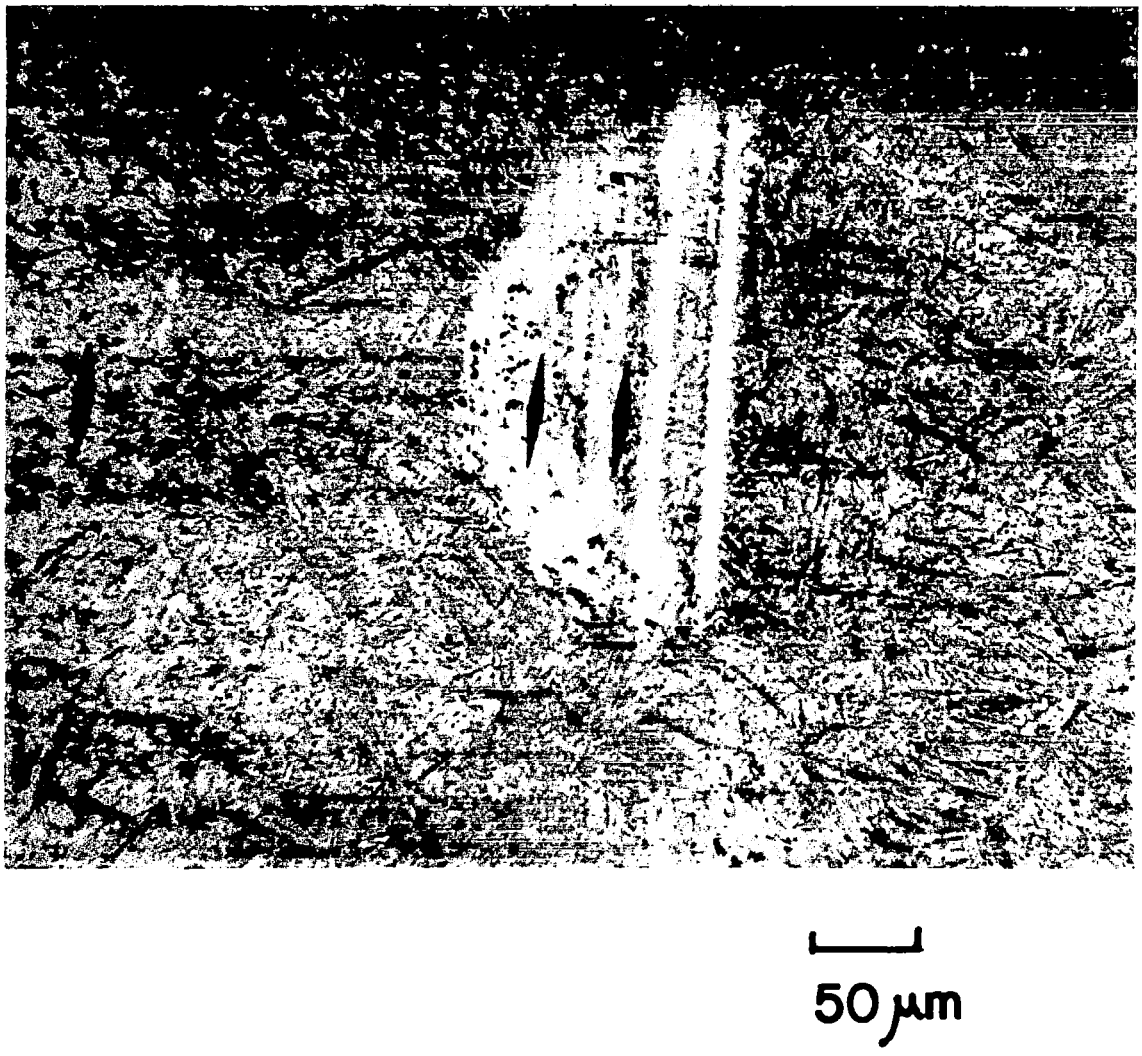

Figure 6.26 Photomicrograph of Scuff Mark After Nital Etching

PART 7

DISCUSSION AND CONCLUSIONS

7.1 Microscopic Contour Changes

The findings of the first set of experiments can be summarized as follows:

1. Scuffed steel bearing surfaces are more reactive toward alcoholic hydrochloric acid than virgin surfaces.
2. Scuffed bearing surfaces originally used on a lubricant containing a small concentration of an organic chloride are much less reactive toward alcoholic hydrochloric acid than surfaces that had become scuffed with the undiluted lubricant.
3. Titanium-nitride-coated steel bearing surfaces did not scuff under conditions where the uncoated surfaces did. They did show track marks, however. Furthermore the coating proved to be porous in general and exhibited a ladder-type structure on the track marks when run with polyphenyl ether containing 1% of 1,1,2-trichloroethane. When run without the chloride, the surface on the track mark was not changed but was just as porous as the virgin surfaces.
4. Uncoated steel bearing surfaces scuffed with polyphenyl ether lubricant containing 1,1,2-trichloroethane showed a high concentration of round specks in the track but only few such specks outside of it. No specks at all were shown when the chloride was absent. These specks are presumably metal chloride.
5. The reactivity of heated metal surfaces toward alcoholic hydrochloric acid at ambient temperature follows an Arrhenius-type relation with temperature. This would seem to indicate that a bearing surface heated to any

one time to a high temperature, e.g., by direct contact, could become much more reactive and therefore perhaps more prone to scuffing at a later time.

The Arrhenius plot of Figure 6.10 would seem to be the result of a lasting change of the metal surface by its reheating or tempering. Perhaps the so-called "chemostress" coefficient defined by Ciftan and Saibel [31] plays a role. These authors have shown a change of chemical potential of an adsorbate with stress in the substrate. The chemical potential expresses the change of free energy change ΔG for a reaction is related to the equilibrium contact K. Therefore, the ratio of a product concentration to that of reactant concentrations, by the well-known thermodynamic relation

$$K = \exp(\Delta G/RT)$$

which is an Arrhenius relation between a product of reaction (e.g., surface profile change) and the absolute temperature can be derived by thermodynamics and continuum mechanics alone. However, the heterogeneity of the metal surface could be the basis of a kinetic explanation: The tempering changes the surface composition logarithmically with temperature because it is diffusion-controlled and the chemical reaction rate depends on the number of reaction sites thereby created. This argument would equally lead to an Arrhenius relation.

Both of these explanations could be valid simultaneously, but the latter seems to be more important on the basis of chemical and especially electrochemical experience. Their relative importance will be determined by repeating the experiments with pure solid surfaces.

Quinn [32] pointed out that the values of the Arrhenius Constant for oxidation during mild (i.e., oxidational) wear are not the same as for oxidation in an oxidizing atmosphere (such as in a furnace). The Arrhenius relation obtained in the previously-mentioned experiment (Figure 6.10) is of the latter type. The reaction rate doubles for every 150°C increase in temperature, and gives improbably low activation energy value. This was pointed out by Dr. Rabinowicz of M.I.T. and he also mentioned that a typical Arrhenius-type process had an activation energy such that the rate of reaction doubled for every 10°C increase in temperature. However, the changes observed actually involve the changes in the surface itself due to the temperature and the addition of the oxide layer which gives a different phase change (see 3.2). Therefore, the complex index of refraction should be measured so that we can separate the two changes.

It was also important to note that titanium-nitride-coated balls barely scuffed under our conditions. Yet, when 1,1,2-trichloroethane was present in the lubricant, the rather remarkable ladder-type structure appeared. The crests at right angles to the direction of ball motion could have been formed in a manner similar to the well-known washboard effect on highway surfaces. In both cases, a liquid was able to creep below the surface as our measurements with the interference microscope indicated and which were confirmed by the scanning electron microscope. The same theory seems to be applicable in both cases.

7.2 Topographical Reaction Rate Measurements

The findings of the second set of experiments can be summarized as follows:

1. Different additives in the base oil have different effects on the surface (Figure 6.14). The subsequent acid treatment on these soaked surfaces have rather different effects. Surface films might have been formed (e.g., phosphate from TCP). The different additives in the lubricant, when combined in the fully-formulated oil, may interact with each other and the result is a totally different reaction and have less roughness changes after the acid treatment.

2. Tricresyl phosphate in lubricant definitely has some effect on the surface. After the TCP-soaked surface was treated by the alcoholic hydrochloric acid, the small asperities were attacked and the large ones remained. If this is not an effect of the chloride or the oxide and the actual surface profiles have this characteristic, this might allow us to gain some insight into how TCP works as an antiwear additive. Hirst and Hollander [33] reported that both the vertical and the horizontal scales of roughness were found to be important, and the authors concluded that from their results that failure occurs as a result of the plastic deformation of those features of the topography that they identify with the main structure of the surface; deformation of the fine structure, of much shorter wavelength, that is superimposed on the main surface is not important. The fact that TCP, as a result of corrosion from the acid treatment, promote the growth of these main structures and might have some influence on its antiwear characteristics.

3. Running the ball/plate contact in PANA or DODPA-containing oil showed that they have worse traction characteristics than the base oil. There is also a higher tendency for

early scuffing in the case of the PANA-containing oil. If these antioxidants prevent the formation of oxide on surfaces, do they actually permit more metal-to-metal contact, thereby promote wear and welding? In the case of the BTZ-containing oil, more severe scuffing is apparent. Is the corrosion inhibitor promoting scuffing even more readily? They all have higher reactivity for long (100 sec or more) operating time. And what kind of interaction goes on between the different additives which allow us to get an apparently better oil? These are all questions to be answered.

4. Soaking of the bearing material for at least 3 hrs prior to operation reduce the reactivity. A possible explanation is that the soaking allows the oil to creep in between the asperities. When the unsoaked metal is run (even though lubrication is provided), the lubricant may not have enough time to get in between the asperities in a matter of a few seconds and therefore causes the contact to run hotter. This might have caused the increase of reactivity and the scuffing.

5. It would seem that a metallurgical change is produced on scuffing and even earlier - though to a smaller extent. This change is long-lasting and responsible for rapid changes of profile on treatment with dilute alcoholic hydrochloric acid. It should be emphasized again that our measurements are carried out on a microscopic scale. The more macroscopic (microscopic in a plane, but not depth-sensitive) metallurgical etching tests showed the presence of a thin layer of a different, and apparently inactive, nonetching phase. It would appear that the new phase of Figure 6.26, which is resistant to etching, is the same or similar to that reported by Rogers [18] for diesel piston rings.

It would appear that steel surfaces approaching or after scuffing, having been exposed to high temperatures, are also much more reactive at ambient temperature, at least toward diluted hydrochloric acid.

Conversely then, such a probe reaction can be very useful to determine scuffing tendencies for different solid materials and lubricants. However, more extensive study is still required before it can be used.

PART 8

LITERATURE CITED

1. O.E.C.D. "Terms and Definitions in Friction, Wear and Lubrication," Metal Research Institute, TNo. Delft, Netherlands.

2. Dyson, A., Tribology, 8, 77-87, 117-121 (1975).

3. Blok, H., J. Soc. Automot. Eng., 44, 193-210, 220 (1939).

4. Lemanski, A.J., Am. Gear Manuf. Assoc., Inf. Sheet No.217.01, 1965.

5. Kelley, B.N. and Lemanski, A.J., Proc. Inst. Mech. En., London, 182, 3A, 178-184 (1967-1968).

6. Ku, P.M., Staph, H.E. and Carper, H.J., USAAMRDL Tech. Rep.75-33, AD AO 13527, Defense Documentation Center, Alexandria, Virginia, 1975.

7. Genkin, M.D., Kuz'min, N.F. and Misharin, Yu.A., In "Izdatelstvo Akademiyi Nauk SSSR, Moscow," Chapter 5. Condensed English translation in National Research Council of Canada, Tech. Transl. 1056, Ottawa, Canada, 1963.

8. Cocks, M. and Tallian, T.E., ASLE Trans. 14, 31-40 (1971).

9. Bell, J.C., Dyson, A. and Hadley, J.W., ASLE Trans., 18, 62-73 (1975).

10. Almen, J.O., In "Mechanical Wear" (J.T. Burwell, ed.), Chapter 12, pp.229-238, American Society for Metals, Metals Park, Ohio, 1948.

11. Bell, J.C. and Dyson, A., Proc. Sym. Elastohydrodynamic Lub., Institution of Mechanical Engineers, London, 1972a, pp.61-67.

12. Leiner, D.C., Master's Thesis, University of Rochester, 1977.

13. Born, M. and Wolf, E., Principles of Optics, 6th ed., pp.627-633, 1980.

14. Blok, H., Measurement of Temperature Flashes on Gear Teeth Under Extreme Pressure Conditions, Proc. Inst. Mech. Eng., General Discussion on Lubricants, Pt.2, pp.14-20, 1937a.

15. Blok, H., Theoretical Study of Temperature Rise on Surfaces of Actual Contact under Lubricating Conditions, Proc. Inst. Mech. Eng., General Discussion on Lubricants, Pt.2, pp.222-231, 1937b.

16. Blok, H., The Constancy of Scoring Temperature, Proc. Interdisciplinary Approach to Lubrication Wear, pp.153-248, 1970. NASA Rep. No.SP-237, Washington, D.C.

17. Merritt, H.E., Gear Engineering, Pitmans, London, 1971.

18. Rogers, M.D., Tribology, 2, 123-127 (1969).

19. Cameron, A., J. Inst. Pet., 37, 471-486 (1951).

20. Cameron, A., Basic Lubrication Theory, 3rd ed., pp.209-210, 1981.

21. Bowden, F.P. and Tabor, D., The Friction and Lubrication of Solids, Oxford University Press (Clarendon), London and New York, 1950,1964.

22. Godfrey, D., ASLE, 8, 1-11 (1965).

23. Shafrin, E.G. and Munday, J.S., ASLE Trans., 21, 4, 329-336 (1978).

24. Goldman, I.B., Wear, 14, 431-444 (1969).

25. Johnson, G.W., Leiner, D.C. and Moore, D.T., Optical Eng., 18, 46-52 (1979).

26. Choi, F.H., Master's Thesis, Rensselaer Polytechnic Institute, 1981.

27. Smith, W.J., Modern Optical Engineering, McGraw-Hill Company, 1966.

28. Lauer, J.L., Keller, L.E., Choi, F.H. and King, V.W., Alignment of Fluid Molecules in an EHD Contact, ASLE Preprint No. 81-LC-5C-1, presented at the ASLE/ASME Lubrication Conference, October 5-7, 1981.

29. Hinterman, H.E. and Boving, H., Wear, 7, 387-398 (1978).

30. Faut, O.D. and Wheeler, D.R., ASLE Preprint No. 820LC-4C-1, presented at the ASME/ASLE Lubrication Conference, October 5-7, 1982.

31. Cifton, M. and Saibel, E., Solid State Communications, 27, 435-437 (1978).

32. Quinn, T.F.J., NASA Interdisciplinary Collaboration in Tribology, A Review of Oxidational Wear, 1983.

33. Hirst, W. and Hollander, A.E., Proc. R. Soc., London, Ser.A337, 379-394 (1974).

1. Report No.	2. Government Accession No.	3. Recipient's Catalog No.
NASA CR-3757		

4. Title and Subtitle	5. Report Date
Surface Topographical Changes Measured by Phase-Locked Interferometry	January 1984
	6. Performing Organization Code
7. Author(s)	8. Performing Organization Report No.
James L. Lauer and Simon S. Fung	None
	10. Work Unit No.
9. Performing Organization Name and Address	11. Contract or Grant No.
Rensselaer Polytechnic Institute Dept. of Mechanical Engineering Troy, New York 12181	NAG3-222
	13. Type of Report and Period Covered
12. Sponsoring Agency Name and Address	Contractor Report
National Aeronautics and Space Administration Washington, D.C. 20546	14. Sponsoring Agency Code 505-36-12 (E-1874)

15. Supplementary Notes

Final report. Project Manager, William R. Jones, Jr., Structures and Mechanical Technologies Division, NASA Lewis Research Center, Cleveland, Ohio 44135.

16. Abstract

An electronic optical laser interferometer capable of resolving depth differences of as low as 30 Å and planar displacements of 6000 Å was constructed for the examination of surface profiles of bearing surfaces without physical contact. This instrument was used to determine topological chemical reactivity by applying a drop of dilute alcoholic hydrochloric acid and measuring the profile of the solid surface before and after application of this probe. It was found that scuffed bearing surfaces reacted much faster than virgin ones but that bearing surfaces exposed to lubricants containing an organic chloride reacted much more slowly. In a separate series of experiments, a number of stainless steel plates were heated in a nitrogen atmosphere to different temperatures and their reactivity examined later at ambient temperature. The change of surface contour as a result of the probe reaction was found to follow an Arrhenius-type relation with respect to heat treatment temperature. In another experiment, the contact area of the plate of a ball/plate (both consisting of hardened M-50 steel) sliding elastohydrodynamic contact run on trimethylolpropane triheptanoate with or without the additives dioctyldiphenylamine (DODPA), phenyl-alpha-naphthylamine (PANA), benzotriazole (BTZ), and tricresyl phosphate (TCP) individually and collectively was optically profiled periodically with the phase-locked interference microscope, both before and after exposure to alcoholic hydrochloric acid. As scuffing was approached the change of profile within the contact region changed much more rapidly by the acid probe and assumed a constant high value after scuffing. A new nonetching metallurgical phase was found in the scuff mark, which was apparently responsible for the high reactivity. Soaking the metal surfaces in the various lubricants before running was found to affect the subsequent reactivity. Based on the above findings, it would appear that this type of examination could be used for screening of potentially scuff-resistant materials.

17. Key Words (Suggested by Author(s))	18. Distribution Statement
Phase-locked interference microscope Tribology	Unclassified - unlimited STAR Category 74

19. Security Classif. (of this report)	20. Security Classif. (of this page)	21. No. of pages	22. Price*
Unclassified	Unclassified	101	A06

*For sale by the National Technical Information Service, Springfield, Virginia 22161

NASA-Langley, 1984